J. Fluid Mech. (2003), *vol.* 496, *pp.* 405–441.
DOI: 10.1017/S0022112003006645 Printed in the United Kingdom

The separated flow of an inviscid fluid around a moving flat plate

By MARVIN A. JONES†

Courant Institute of Mathematical Sciences, New York University, 251 Mercer St., New York, NY 10012, USA

(Received 3 September 2002 and in revised form 19 August 2003)

In this study we consider the separated flow of an inviscid fluid around a moving flat plate. The motion of the plate, which is initially started from rest, is prescribed and unconstrained and we set ourselves the task of fully characterizing the resulting motion in the surrounding fluid. To do this we use a boundary integral representation for the complex-conjugate velocity field $\Phi(z,t)$ and require that the force and torque on the plate be determined as part of the solution. The flow solution is assumed to consist of a bound vortex sheet coincident with the plate and two free vortex sheets that emanate from each of the plate's two sharp edges. The time evolution of these vortex sheets is then considered in general. For physical reasons, the flow solution is required to satisfy the unsteady Kutta condition, which states that $\Phi(z,t)$ must be bounded everywhere, and the rigorous imposition of this condition then yields two types of additional constraint. The first governs the rate at which circulation is shed from the plate's edges and the second ensures that the free vortex sheets are shed tangentially. In fact, all the familiar flow characteristics associated with the imposition of the steady Kutta condition are rigorously shown to have exact parallels in the unsteady case. In addition, explicit expressions for the normal force and torque on the plate are derived. An asymptotic solution to the full system of evolution equations is developed for small times $t > 0$ and a simplified version of this solution is used as an initial condition for a desingularized numerical treatment of the full problem. A fast numerical algorithm is proposed and implemented and the results of several example calculations are presented. The featured examples are limited to high effective angles of attack due to the occurrence of a specific type of event that prevents further time-integration of the evolution equations using the current numerical method. The event corresponds physically to a situation in which a Lagrangian point placed at one of the plate's edges moves onto instead of away from the edge.

1. Introduction

Here the problem of determining the unsteady separated flow of an inviscid fluid around a moving flat plate is considered and solved in two dimensions using a boundary integral representation for the complex-conjugate velocity field. It is assumed that the fluid motion is entirely induced by the plate's motion, which is started from rest.

† Present address: Department of Applied Mathematics and Theoretical Physics, University of Cambridge, Centre for Mathematical Sciences, Wilberforce Road, Cambridge CB3 0WA UK.

The problem is one of fundamental importance in unsteady fluid dynamics since an understanding of the complicated processes of unsteady separation and vortex shedding is required in order to determine its solution. A complete mathematical description of these phenomena, at finite Reynolds number, would of course require that the detailed effects of viscosity be taken into account. However, in the limit of infinite Reynolds number it is possible to successfully model the fluid's motion using a purely inviscid theory in which the processes of separation and vortex shedding are included; this is the approach taken here.

The effects of viscosity are included by allowing discontinuous solutions of the governing Euler equations, in particular solutions containing vortex sheets. Such solutions are considered physically acceptable since the presence of viscosity, however small, leads to the smoothing of these discontinuities in a real fluid. On the other hand, solutions containing singularities are considered unphysical and the condition which states that the fluid's velocity be bounded everywhere is rigorously imposed. This condition is referred to as the unsteady Kutta condition as it is related to the well-known Kutta condition, which has been successfully applied in many areas of steady fluid mechanics for many years.

In practice, the steady Kutta condition is routinely imposed in a number of different forms and this has led to some confusion concerning its use in the unsteady case. In an attempt to bring some clarity to the subject, the current study shows that all the familiar conditions associated with the imposition of the steady Kutta condition have corresponding conditions in the unsteady case. Furthermore, the current study shows rigorously that all these conditions can be derived from the central physical principle which states that the velocity field should be bounded everywhere. This emphasis is not new. Indeed, the inspirational work of Pullin (1978) placed central importance on the principle with impressive results.

Another source of confusion with regard the use of the unsteady Kutta condition has been the plethora of different methods that have been invented to impose it numerically. As Sarpkaya (1989) remarked in his excellent review article, 'almost every paper, at least in part, represents a new method'. For example, most authors, including Kuwahara (1973), Clements (1973), Sarpkaya (1975), Katz (1981), and Cortelezzi, Cheng & Chan (1997), have chosen to model the continual shedding of vorticity from a sharp edge by introducing a new vortex element into the flow at the beginning of each time step. The strength, position, and velocity of the 'nascent' vortex elements are then chosen, more or less arbitrarily, to satisfy the authors chosen version of the unsteady Kutta condition and this has sometimes led to spurious results. Indeed, disturbingly large errors have been reported in comparison with the experimental data of Fage & Johansen (1927), Keulegan & Carpenter (1958), Taneda & Honji (1971), and Pullin & Perry (1980).

In the work of Krasny (1991) and Nitsche & Krasny (1994) the vortex elements are released exactly at the edge, instead of being placed into the flow at some arbitrary location. As a result their comparison with the experimental work of Didden (1979), as presented in Nitsche & Krasny (1994), is compelling. However, some arbitrary choices still remain in the details of the shedding procedure used. The current study seeks to completely circumvent all of these issues by, once again, placing singular emphasis on the physical principle that the velocity field should be bounded everywhere. Once this condition is imposed analytically, there is no need to invent a new numerical method; the shedding procedure is handled in a completely natural way.

At this point, it is worth pointing out that the boundary integral formulation used in the forthcoming analysis is preferred to an equivalent formulation based on

conformal mapping theory (most previous authors have used conformal mapping theory) for two reasons. First, a method based on conformal mapping could not be generalized in order to tackle three-dimensional problems, whereas the boundary integral formulation used here shows promise in this respect. And second, although the current study concerns only to the motion of a rigid flat plate, it is envisaged that the theory developed here will be extended to cover the corresponding motion of a flexible object, a situation that is most naturally modelled using a boundary integral formulation.

To summarize, the attached potential flow solution for the problem under consideration has a singular velocity field at each of the plate's two sharp edges and is therefore physically unacceptable. However, if we allow separation at both of the plate's edges then the velocity field can be renormalized and the unsteady Kutta condition satisfied analytically. In fact, in order to satisfy the unsteady Kutta condition at all times, whatever the motion of the plate, the flow solution must be allowed the freedom to contort in various ways. And it is with these contortions that we are primarily concerned. However, it is first necessary to develop a general approach.

2. Problem formulation

We choose to pose the problem in the rest frame of the fluid in the far field and the complex number $z = x + \mathrm{i}y$ is used to denote the position of a point in this frame, where x and y are the horizontal and vertical Cartesian coordinates of the point z. We assume that the flat plate under consideration is made to execute some predetermined rigid-body motion relative to this frame of reference and our task then becomes one of determining the force and torque on the plate as well as the resulting motion of the surrounding fluid.

For now, we will assume that the flow separates from each of the plate's edges, giving rise to two free shear layers in the flow. Since the Reynolds number is assumed infinite the separated shear layers do not diffuse and thicken, but remain thin for all time. As a result we can successfully model the fluid's motion by replacing the flat plate with a bound vortex sheet and the two free shear layers with two free vortex sheets. The motions of these vortex sheets are then considered. We remind the reader that a vortex sheet is a line discontinuity in the fluid across which the normal component of fluid velocity is continuous, whereas the tangential component of velocity is discontinuous.

The position of the bound vortex sheet, denoted $l_{=}(t)$, is known since it coincides with that of the plate at time t. However, the positions of the free vortex sheets, denoted $l_{+}(t)$ and $l_{-}(t)$, are assumed known only initially and must be found as part of the solution at later times. The edges of the plate from which the free vortex sheets $l_{\pm}(t)$ emanate are denoted $c_{\pm}(t)$ and the centre of the plate is denoted $c(t)$. See figure 1.

The three connected vortex sheets are collectively denoted $l(t)$ and the complex number ζ is used to denote the position of a point on $l(t)$. Since the vortex sheets are connected it is possible to define the arclength, denoted $s(\zeta, t)$, as the distance along $l(t)$ from $c(t)$ to ζ. We note that

$$s(\zeta, t) = (\zeta - c)\,\mathrm{e}^{-\mathrm{i}\theta(t)} \quad \text{for} \quad \zeta \in l_{=}(t), \tag{2.1}$$

since $l_{=}(t)$ is a straight line segment. In (2.1) $\theta(t)$ has been introduced to denote the angle that the plate makes with the horizontal and we will also use $\theta_{\pm}(\zeta, t)$ to denote the angle that the tangent vector to $l_{\pm}(t)$ makes with the horizontal at the point ζ.

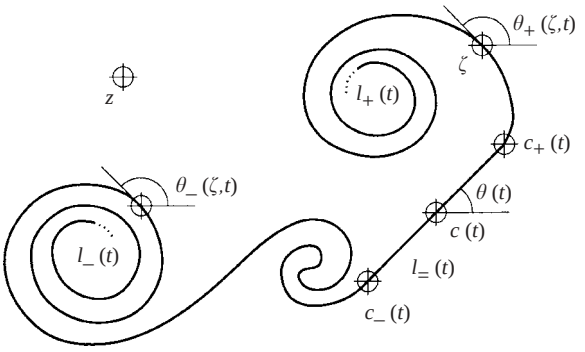

FIGURE 1. A diagram of the flat plate $l_=(t)$, its two trailing vortex sheets $l_\pm(t)$, the points z, ζ, $c(t)$, and $c_\pm(t)$, and the angles $\theta(t)$ and $\theta_\pm(\zeta,t)$ at some time $t>0$.

All tangent vectors are assumed to point in the $s(\zeta,t)$-increasing direction. In order to simplify the forthcoming analysis we also set $s(c_\pm,t)=\pm 1$ and as a result we must have

$$c_\pm(t) = c(t) \pm \mathrm{e}^{\mathrm{i}\theta(t)}. \tag{2.2}$$

This effectively non-dimensionalizes the problem based on one-half of the plate's chord length and we denote this reference length as L. The reference velocity, denoted U, is taken to be the typical velocity of a point fixed in the plate. The plate can be made to perform arbitrary rigid-body motions by controlling the position of $c(t)$ and the angle $\theta(t)$.

The question of how the free vortex sheets come into existence, assuming the motion is started from rest, is an important one and will be considered in detail in § 4. However, the fact that the motion is started from rest implies that any vorticity in the flow must have been created within the bound vortex sheet, $l_=(t)$, and as a result either remains on $l_=(t)$ or is shed into one of the free vortex sheets, $l_\pm(t)$. It therefore follows that most of the fluid is free from vorticity for all time and so the task of solving the governing Euler equations becomes the simplified task of solving the equations of potential flow. In fact, if we choose to represent the flow in terms of the complex-conjugate velocity field, denoted $\Phi(z,t)=u(z,t)-\mathrm{i}v(z,t)$ where $u(z,t)$ and $v(z,t)$ are the horizontal and vertical components of the fluid velocity respectively, then our task becomes one of finding a sectionally holomorphic function $\Phi(z,t)$ that is discontinuous across $l(t)$, that vanishes in the far field, that satisfies the appropriate normal velocity boundary conditions on the plate, and that is bounded everywhere.

In order to automatically satisfy the first three of these conditions we choose to write $\Phi(z,t)$ as a boundary integral of the form

$$\Phi(z,t) = \frac{1}{2\pi\mathrm{i}}\left[\int_{l_-(t)} \frac{\phi_-(\lambda,t)}{(\lambda-z)}\,\mathrm{d}\lambda + \int_{l_=(t)} \frac{\phi_=(\lambda,t)}{(\lambda-z)}\,\mathrm{d}\lambda + \int_{l_+(t)} \frac{\phi_+(\lambda,t)}{(\lambda-z)}\,\mathrm{d}\lambda\right], \tag{2.3}$$

where $\phi_-(\zeta,t)$, $\phi_=(\zeta,t)$, and $\phi_+(\zeta,t)$ are the complex vortex sheet strengths associated with the vortex sheets $l_-(t)$, $l_=(t)$, and $l_+(t)$ respectively. The free vortex sheet strengths $\phi_\pm(\zeta,t)$ are known only initially and must be found as part of the solution at later times. In contrast, the bound vortex sheet strength $\phi_=(\zeta,t)$ is unknown initially and must be found as part of the solution at every instant in time.

At first glance, it may seem over complicated to split the boundary integral in equation (2.3) into its three constituent parts. However, at this stage no relations between the angles $\theta(t)$ and $\theta_{\pm}(c_{\pm}, t)$ or the vortex sheet strengths $\phi_{=}(c_{\pm}, t)$ and $\phi_{\pm}(c_{\pm}, t)$ have been imposed, and to emphasize this fact equation (2.3) is preferred.

We continue by imposing some of the more straightforward boundary conditions on $\Phi(z, t)$ so that subsequent definitions can be made. First, since $\Phi(z, t)$ is discontinuous across $l(t)$, it is necessary to derive expressions for the limiting values of $\Phi(z, t)$ as z approaches $l(t)$ from the right and the left. The right and left of $l(t)$ are defined relative to a person standing on $l(t)$ facing in the direction of increasing arclength. Fortunately, the expressions for these limiting values are well known as the Plemelj formulae and, when applied to equation (2.3), state that

$$\Phi_{=}^{\pm}(\zeta, t) = \frac{1}{2\pi \mathrm{i}} \left[\int_{l_{-}(t)} \frac{\phi_{-}(\lambda, t)}{(\lambda - \zeta)} \, \mathrm{d}\lambda + \int_{l_{=}(t)} \frac{\phi_{=}(\lambda, t)}{(\lambda - \zeta)} \, \mathrm{d}\lambda + \int_{l_{+}(t)} \frac{\phi_{+}(\lambda, t)}{(\lambda - \zeta)} \, \mathrm{d}\lambda \right] \pm \tfrac{1}{2} \phi_{=}(\zeta, t), \quad (2.4)$$

where $\Phi_{=}^{-}(\zeta, t)$ and $\Phi_{=}^{+}(\zeta, t)$ are the values of $\Phi(z, t)$ on the right and left of $l_{=}(t)$ at ζ respectively. Similar expressions hold for $\Phi_{\pm}^{\pm}(\zeta, t)$ on $l_{\pm}(t)$. In (2.4) the integral over $l_{=}(t)$ is defined in the sense of a Cauchy principal value and the reader will note that no specific notation is used to highlight the presence of the principal value integral. If this causes confusion the reader is advised to consider all integrals as principal value integrals and is assured that this approach will always lead to the correct result. Armed with equation (2.4) it becomes straightforward to impose the boundary condition which states that the normal component of the velocity is continuous across $l_{=}(t)$. In doing so we find that

$$\phi_{=}(\zeta, t) = \gamma_{=}(\zeta, t) \, \mathrm{e}^{-\mathrm{i}\theta(t)}, \quad (2.5)$$

where $\gamma_{=}(\zeta, t)$ is a real function that measures the jump in tangential velocity across $l_{=}(t)$. Similar arguments apply on the free vortex sheets and we find that

$$\phi_{\pm}(\zeta, t) = \gamma_{\pm}(\zeta, t) \, \mathrm{e}^{-\mathrm{i}\theta_{\pm}(\zeta, t)}, \quad (2.6)$$

where $\gamma_{\pm}(\zeta, t)$ are real functions that measure the jump in tangential velocity across $l_{\pm}(t)$. Noting that $\phi_{=}(\zeta, t)$ and $\phi_{\pm}(\zeta, t)$ take the forms given in equations (2.5) and (2.6) allows us to define the real function $\Gamma(\zeta, t)$ in the form

$$\Gamma(\zeta, t) = \begin{cases} \displaystyle\int_{l_{-}(\zeta, t)} \phi_{-}(\lambda, t) \, \mathrm{d}\lambda & \text{for} \quad \zeta \in l_{-}(t) \\ \displaystyle\int_{l_{=}(\zeta, t)} \phi_{=}(\lambda, t) \, \mathrm{d}\lambda + \Gamma_{-}(t) & \text{for} \quad \zeta \in l_{=}(t) \\ \displaystyle\int_{l_{+}(\zeta, t)} \phi_{+}(\lambda, t) \, \mathrm{d}\lambda + \Gamma_{+}(t) & \text{for} \quad \zeta \in l_{+}(t), \end{cases} \quad (2.7)$$

where $l_{=}(\zeta, t)$ is the portion of $l_{=}(t)$ up to and including the point ζ. The function $\Gamma(\zeta, t)$ is commonly referred to as the circulation in the sheet $l(\zeta, t)$ but is strictly the negative of the circulation around a closed contour that intersects $l(t)$ exactly once at ζ and encloses the free end of $l_{-}(t)$. Such a contour is shown in figure 2. Furthermore, Kelvin's circulation theorem states that if the flow is started from rest then the total circulation around a closed contour that does not intersect $l(t)$ must be zero for all

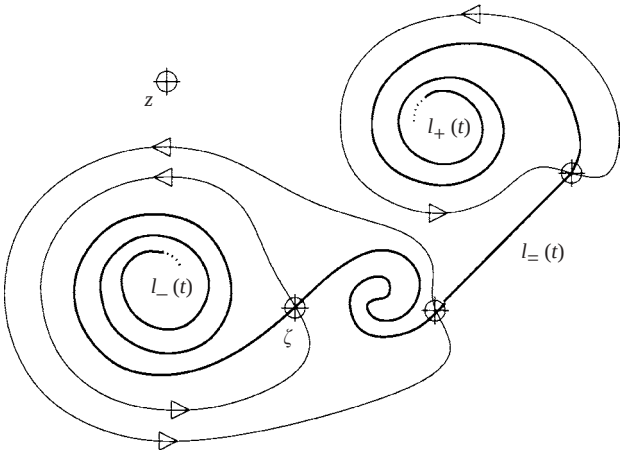

FIGURE 2. A diagram of the flat plate $l_=(t)$, its two trailing vortex sheets $l_\pm(t)$, and the closed contours that are used to define the circulations $\Gamma(\zeta, t)$ and $\Gamma_\pm(t)$ at some time $t > 0$.

time. To satisfy Kelvin's theorem and to ensure that $\Gamma(\zeta, t)$ is a continuous function of ζ we must satisfy the additional constraints

$$\Gamma_-(t) = \int_{l_-(t)} \phi_-(\lambda, t)\,\mathrm{d}\lambda, \tag{2.8}$$

$$\Gamma_+(t) - \Gamma_-(t) = \int_{l_=(t)} \phi_=(\lambda, t)\,\mathrm{d}\lambda, \tag{2.9}$$

$$\Gamma_+(t) = -\int_{l_+(t)} \phi_+(\lambda, t)\,\mathrm{d}\lambda. \tag{2.10}$$

In (2.8)–(2.10) $\Gamma_+(t)$ denotes the circulation around a closed contour that encloses the whole of $l_+(t)$ and nothing else. Similarly, $\Gamma_-(t)$ denotes the negative of the circulation around a closed contour that encloses the whole of $l_-(t)$ and nothing else. Two such contours are also shown in figure 2. Since $\phi_\pm(\zeta, t)$ are known initially it follows, from equations (2.8) and (2.10), that the circulations $\Gamma_\pm(t)$ are also known initially. However, $\Gamma_\pm(t)$ must be found as part of the solution at later times.

To complete our preparatory definitions we note that it is often helpful to write $\Phi(z, t)$ in an alternative form to that shown in equation (2.3). If we parameterize the integrals over $l_\pm(t)$ in terms of the circulation $\Gamma(\zeta, t)$ and take advantage of the fact that $\mathrm{d}\Gamma = \phi_\pm(\zeta, t)\,\mathrm{d}\zeta$ on $l_\pm(t)$ then we can rewrite $\Phi(z, t)$ in the form

$$\Phi(z, t) = \frac{1}{2\pi\mathrm{i}}\left[\int_0^{\Gamma_-(t)} \frac{\mathrm{d}\Lambda}{(\zeta_-(\Lambda, t) - z)} + \int_{l_=(t)} \frac{\phi_=(\lambda, t)}{(\lambda - z)}\,\mathrm{d}\lambda - \int_0^{\Gamma_+(t)} \frac{\mathrm{d}\Lambda}{(\zeta_+(\Lambda, t) - z)}\right], \tag{2.11}$$

where $\zeta_\pm(\Gamma, t)$ denotes the position of the point on $l_\pm(t)$ at which the circulation is equal to Γ. The alternative form for $\Phi(z, t)$ is useful because it clearly shows that $\Phi(z, t)$ depends explicitly on $\Gamma_\pm(t)$ through the upper limits of integration in equation (2.11). We are now in a position to impose the remaining boundary conditions.

3. General solution

First, we choose to impose the kinematic boundary condition, which states that the normal component of the fluid velocity on either side of the plate must be the same as the normal component of the plate's velocity. This condition can be stated in the form $\mathrm{Re}\{(\Phi_{=}^{+}(\zeta,t)+\Phi_{=}^{-}(\zeta,t))\,\mathrm{i}\,\mathrm{e}^{\mathrm{i}\theta(t)}\}=2\nu(\zeta,t)$ for $\zeta\in l_{=}(t)$ where

$$\nu(\zeta,t)=\eta(t)+\dot{\theta}(t)s(\zeta,t) \tag{3.1}$$

is the normal component of the velocity of the plate, $\eta(t)=\mathrm{Im}\{\dot{c}(t)\,\mathrm{e}^{-\mathrm{i}\theta(t)}\}$, and a dot indicates differentiation with respect to time. Substitution of $\Phi_{=}^{\pm}(\zeta,t)$ into the above condition, using the Plemelj formulae as applied to equation (2.11), yields the singular Fredholm integral equation of the first kind

$$\frac{\mathrm{e}^{\mathrm{i}\theta(t)}}{\pi}\int\limits_{l_{=}(t)}\frac{\phi_{=}(\lambda,t)}{(\lambda-\zeta)}\,\mathrm{d}\lambda=f(\zeta,t)\quad\text{for}\quad\zeta\in l_{=}(t), \tag{3.2}$$

which must be solved for the $\phi_{=}(\zeta,t)$ subject to the constraint (2.9). The left-hand side of equation (3.2) is purely real, as can be seen by parameterizing the integral in terms of arclength using equations (2.1) and (2.5), and the right-hand side takes the form

$$f(\zeta,t)=2\nu(\zeta,t)-2\mathrm{Re}\left\{\frac{\mathrm{e}^{\mathrm{i}\theta(t)}}{2\pi}\left[\int\limits_{0}^{\Gamma_{-}(t)}\frac{\mathrm{d}\Lambda}{(\zeta_{-}(\Lambda,t)-\zeta)}-\int\limits_{0}^{\Gamma_{+}(t)}\frac{\mathrm{d}\Lambda}{(\zeta_{+}(\Lambda,t)-\zeta)}\right]\right\}. \tag{3.3}$$

Fortunately, the exact inversion formula for equation (3.2) is available from Muskhelishvili (1946, p. 249). However, the inversion formula is, in general, non-unique and the relevant solution must usually be chosen by specifying the behaviour of the solution at the ends of $l_{=}(t)$ and in the far field. Thankfully, no such arbitrary choice is necessary here since in order to automatically satisfy the constraint (2.9) we must write the solution for $\phi_{=}(\zeta,t)$ in the form

$$\phi_{=}(\zeta,t)=\frac{-(\pi\mathrm{i})^{-1}}{\sqrt{\zeta-c_{+}}\sqrt{\zeta-c_{-}}}\left[\Gamma_{+}(t)-\Gamma_{-}(t)+\mathrm{i}\,\mathrm{e}^{-\mathrm{i}\theta(t)}\int\limits_{l_{=}(t)}\frac{\sqrt{\lambda-c_{+}}\sqrt{\lambda-c_{-}}}{(\lambda-\zeta)}f(\lambda,t)\,\mathrm{d}\lambda\right], \tag{3.4}$$

where the time dependence of $c_{\pm}(t)$ has been omitted for clarity.

We note that $\phi_{=}(\zeta,t)$ is, in general, unbounded at $\zeta=c_{\pm}(t)$, having inverse square-root singularities there. To aid in the forthcoming analysis, it is therefore useful to rewrite $\phi_{=}(\zeta,t)$ in a form that explicitly separates out the singular terms in $\phi_{=}(\zeta,t)$ from the non-singular ones. This decomposition is performed in two stages. First, we identify the singular behaviour of $f(\zeta,t)$ as logarithmic by rewriting equation (3.3) in the form

$$\begin{aligned}f(\zeta,t)=2\nu(\zeta,t)&+\frac{1}{\pi}\mathrm{Re}\{\phi_{+}(c_{+},t)\log(\zeta-c_{+})\,\mathrm{e}^{\mathrm{i}\theta(t)}\}\\&-\frac{1}{\pi}\mathrm{Re}\{\phi_{-}(c_{-},t)\log(\zeta-c_{-})\,\mathrm{e}^{\mathrm{i}\theta(t)}\}-2\mathrm{Re}\{\psi(\zeta,t)\},\end{aligned} \tag{3.5}$$

where $\psi(\zeta, t)$ is a well-behaved bounded function of the form

$$\psi(\zeta,t)=\frac{e^{i\theta(t)}}{2\pi}\left[\phi_+(c_+,t)\log(\zeta-c_+)-\int_0^{\Gamma_+(t)}\frac{d\Lambda}{(\zeta_+(\Lambda,t)-\zeta)}\right.$$
$$\left.-\phi_-(c_-,t)\log(\zeta-c_-)+\int_0^{\Gamma_-(t)}\frac{d\Lambda}{(\zeta_-(\Lambda,t)-\zeta)}\right]. \quad (3.6)$$

Second, we substitute equations (3.1), (3.5), and (3.6) into equation (3.4), interchange the order of integration in the resulting double integrals, and evaluate the remaining integrals over $l_=(t)$ exactly using the identities listed in Appendix A. Having completed these tasks we eventually obtain $\phi_=(\zeta, t)$ in the form

$$\phi_=(\zeta,t)=\frac{1}{\pi}\left[\frac{(A(t)+B(t)s(\zeta,t))}{r(\zeta,t)}-C(\zeta,t)r(\zeta,t)+D(\zeta,t)\right]e^{-i\theta(t)}, \quad (3.7)$$

where

$$A(t)=\pi\dot\theta(t)+\int_0^{\Gamma_+(t)}\mathrm{Re}\left\{\frac{(\zeta_+(\Lambda,t)-c)}{\sqrt{\zeta_+(\Lambda,t)-c_+}\sqrt{\zeta_+(\Lambda,t)-c_-}}\right\}d\Lambda$$
$$-\int_0^{\Gamma_-(t)}\mathrm{Re}\left\{\frac{(\zeta_-(\Lambda,t)-c)}{\sqrt{\zeta_-(\Lambda,t)-c_+}\sqrt{\zeta_-(\Lambda,t)-c_-}}\right\}d\Lambda, \quad (3.8)$$

$$B(t)=2\pi\eta(t)+\int_0^{\Gamma_+(t)}\mathrm{Re}\left\{\frac{e^{i\theta(t)}}{\sqrt{\zeta_+(\Lambda,t)-c_+}\sqrt{\zeta_+(\Lambda,t)-c_-}}\right\}d\Lambda$$
$$-\int_0^{\Gamma_-(t)}\mathrm{Re}\left\{\frac{e^{i\theta(t)}}{\sqrt{\zeta_-(\Lambda,t)-c_+}\sqrt{\zeta_-(\Lambda,t)-c_-}}\right\}d\Lambda, \quad (3.9)$$

and

$$C(\zeta,t)=2\pi\dot\theta(t)+\int_0^{\Gamma_+(t)}\mathrm{Re}\left\{\frac{e^{2i\theta(t)}}{\sqrt{\zeta_+(\Lambda,t)-c_+}\sqrt{\zeta_+(\Lambda,t)-c_-}(\zeta_+(\Lambda,t)-\zeta)}\right\}d\Lambda$$
$$-\int_0^{\Gamma_-(t)}\mathrm{Re}\left\{\frac{e^{2i\theta(t)}}{\sqrt{\zeta_-(\Lambda,t)-c_+}\sqrt{\zeta_-(\Lambda,t)-c_-}(\zeta_-(\Lambda,t)-\zeta)}\right\}d\Lambda$$
$$-\frac{D(\zeta,t)}{i\sqrt{\zeta-c_+}\sqrt{\zeta-c_-}e^{-i\theta(t)}}, \quad (3.10)$$

are purely real, as is $r(\zeta,t)=-i\sqrt{\zeta-c_+}\sqrt{\zeta-c_-}e^{-i\theta(t)}$.

Before continuing we remark that the real function $D(\zeta, t)$ is effectively arbitrary and can be set to zero without affecting the validity of equations (3.7)–(3.10). However, it is possible to choose $D(\zeta, t)$ so that both $C(\zeta, t)$ and $D(\zeta, t)$ are well behaved bounded functions of ζ that, in particular, approach well-defined limits as $\zeta \to c_\pm(t)$. This is important since it shows that equation (3.7) is a sensible and useful

decomposition of $\phi_{=}(\zeta, t)$. To accomplish this we choose $D(\zeta, t)$ in the form

$$D(\zeta, t) = \pi\phi_{+}(c_{+}, t)a_{+}(s(\zeta, t))\,\mathrm{e}^{\mathrm{i}\theta(t)} + \pi\phi_{-}(c_{-}, t)a_{-}(s(\zeta, t))\,\mathrm{e}^{\mathrm{i}\theta(t)}, \tag{3.11}$$

where

$$a_{\pm}(s) = \left(1 - \frac{1}{\pi}\arccos(\pm s)\right)\mathrm{Re}\{\mathrm{e}^{\mathrm{i}\chi_{\pm}(t)}\}\,\mathrm{e}^{-\mathrm{i}\chi_{\pm}(t)}. \tag{3.12}$$

We also note that the quantities $\chi_{\pm}(t) = \theta(t) - \theta_{\pm}(c_{\pm}, t)$ in (3.12) represent the angles between the plate and the tangents to $l_{\pm}(t)$ at $c_{\pm}(t)$. These quantities are non-zero in general.

3.1. *Removing the inverse square-root singularities in $\Phi(z, t)$*

Having found the bound vortex sheet strength in the form (3.7), we are finally faced with the task of imposing the boundedness of $\Phi(z, t)$. To accomplish this it is first necessary to understand in detail how the behaviour of the vortex sheet strengths $\phi_{=}(\zeta, t)$ and $\phi_{\pm}(\zeta, t)$ influence the behaviour of the complex-conjugate velocity field $\Phi(z, t)$ through equation (2.3). Fortunately, the results we will need to gain this understanding are well known and can again be found in Muskhelishvili (1946, chap. 4). They concern the behaviour of Cauchy integrals near the ends of the line of integration and the relevant results are reproduced in Appendix B for convenience.

The results restated in Appendix B show, when applied to equations (2.3) and (3.7), that the inverse square-root singularities in $\phi_{=}(\zeta, t)$ at $\zeta = c_{\pm}(t)$ lead to corresponding inverse square-root singularities in $\Phi(z, t)$ at $z = c_{\pm}(t)$. This is physically unacceptable and it is clear that if $\Phi(z, t)$ is to remain bounded then the inverse square-root singularities in $\phi_{=}(\zeta, t)$ must first be removed.

Equations (2.2) and (3.7) show that in order to remove the unwanted singularities we must satisfy the additional constraints $A(t) \pm B(t) = 0$, which effectively set $A(t) = B(t) = 0$. When written out in full these constraints take the form

$$\pi\dot{\theta}(t) \pm 2\pi\eta(t) + \int_{0}^{\Gamma_{+}(t)} \mathrm{Re}\left\{\frac{\sqrt{\zeta_{+}(\Lambda, t) - c_{\mp}}}{\sqrt{\zeta_{+}(\Lambda, t) - c_{\pm}}}\right\}\mathrm{d}\Lambda - \int_{0}^{\Gamma_{-}(t)} \mathrm{Re}\left\{\frac{\sqrt{\zeta_{-}(\Lambda, t) - c_{\mp}}}{\sqrt{\zeta_{-}(\Lambda, t) - c_{\pm}}}\right\}\mathrm{d}\Lambda = 0. \tag{3.13}$$

Moreover, the constraints in (3.13) can be solved simultaneously for the unknown circulations $\Gamma_{\pm}(t)$, thereby determining the amount of circulation in each of the free vortex sheets at each instant in time. Equations (3.13) prove very useful, both from an analytical and numerical perspective. However, they are unconventional and can be replaced by an equivalent set of first-order ordinary differential equations for $\dot{\Gamma}_{\pm}(t)$. To derive these ordinary differential equations we begin by rewriting (3.13) in the form

$$\lim_{\epsilon \to 0}\left[\int_{0}^{\Gamma_{\pm}(t) - \epsilon} \alpha_{\pm}(\Lambda, t)\,\mathrm{d}\Lambda\right] = \beta_{\pm}(t),$$

where

$$\alpha_{\pm}(\Gamma, t) = \mathrm{Re}\left\{\frac{\sqrt{\zeta_{\pm}(\Gamma, t) - c_{\mp}}}{\sqrt{\zeta_{\pm}(\Gamma, t) - c_{\pm}}}\right\},$$

and

$$\beta_{\pm}(t) = \mp\pi\dot{\theta}(t) - 2\pi\eta(t) + \int_0^{\Gamma_{\mp}(t)} \mathrm{Re}\left\{\frac{\sqrt{\zeta_{\mp}(\Lambda,t)-c_{\mp}}}{\sqrt{\zeta_{\mp}(\Lambda,t)-c_{\pm}}}\right\}\mathrm{d}\Lambda.$$

The upper limit of integration in the first of the three equations above has been modified to temporarily avoid problems associated with the inverse square-root singularity in the integrand $\alpha_{\pm}(\Gamma,t)$ at $\Gamma=\Gamma_{\pm}(t)$. The singularity exists since $\zeta_{\pm}(\Gamma_{\pm}(t),t)=c_{\pm}(t)$ by definition and we note that there is no such singularity in the integrand appearing in the definition of $\beta_{\pm}(t)$. We continue by differentiating both sides of the rewritten constraints with respect to time. The order in which the time derivative and the limit $\epsilon\to 0$ are taken is reversed and the formula for the derivative of an integral containing a time-dependent limit of integration is used. After the addition and subtraction of an arbitrary flux integral we obtain

$$\lim_{\varepsilon\to 0}\left[\alpha_{\pm}(\Gamma_{\pm}(t)-\epsilon,t)(\dot{\Gamma}_{\pm}(t)-\delta_{\pm}(\Gamma_{\pm}(t)-\epsilon,t))\right.$$
$$\left.+\alpha_{\pm}(0,t)\delta_{\pm}(0,t)+\int_0^{\Gamma_{\pm}(t)-\epsilon}\frac{\partial\alpha_{\pm}}{\partial t}(\Lambda,t)+\frac{\partial}{\partial\Lambda}(\alpha_{\pm}(\Lambda,t)\delta_{\pm}(\Lambda,t))\,\mathrm{d}\Lambda\right]=\dot{\beta}_{\pm}(t),$$

where the derivative on the right-hand side can be obtained explicitly from the definition of $\beta_{\pm}(t)$ without difficulty. We note two things about the above equation. First, the term $\alpha_{\pm}(\Gamma_{\pm}(t)-\epsilon,t)(\dot{\Gamma}_{\pm}(t)-\delta_{\pm}(\Gamma_{\pm}(t)-\epsilon,t))$ has the potential to become singular as $\epsilon\to 0$. And second, the remaining terms are non-singular and can be made to exactly cancel by choosing the arbitrary function $\delta_{\pm}(\Gamma,t)$ to be

$$\delta_{\pm}(\Gamma,t)=\frac{1}{\alpha_{\pm}(\Gamma,t)}\left[\dot{\beta}_{\pm}(t)-\int_0^{\Gamma}\frac{\partial\alpha_{\pm}}{\partial t}(\Lambda,t)\,\mathrm{d}\Lambda\right].$$

By construction, we are then left with a limiting relation that effectively sets $\dot{\Gamma}_{\pm}(t)$ equal to $\lim_{\epsilon\to 0}[\delta_{\pm}(\Gamma_{\pm}(t)-\epsilon,t)]$ and all that remains is to evaluate this limit.

Use of integration by parts in the definition of $\delta_{\pm}(\Gamma,t)$, followed by a partial evaluation of the limit $\epsilon\to 0$, allows us to express the limit under investigation in terms of the partial derivatives of $\alpha_{\pm}(\Gamma,t)$. And subsequent evaluation of these partial derivatives, using equations (2.1), (2.2), and the definition of $\alpha_{\pm}(\Gamma,t)$, followed by the final evaluation of the limit $\epsilon\to 0$ then leads to the result

$$\lim_{\epsilon\to 0}[\delta_{\pm}(\Gamma_{\pm}(t)-\epsilon,t)]=-\left[\frac{\partial s_{\pm}}{\partial t}(\Gamma_{\pm}(t),t)\Big/\frac{\partial s_{\pm}}{\partial\Gamma}(\Gamma_{\pm}(t),t)\right],$$

in which the notation $s_{\pm}(\Gamma,t)$ has been introduced to denote the arclength at which the circulation is equal to Γ.

Further progress is possible if we notice two more things. First, the denominator in the above equation is equal to the reciprocal of $\phi_{\pm}(c_{\pm},t)\exp(\mathrm{i}(\theta(t)-\chi_{\pm}(t)))$. And second, the numerator represents the speed of a Lagrangian point on $l_{\pm}(t)$ at $c_{\pm}(t)$ as measured relative to $c_{\pm}(t)$. Since these Lagrangian points are labelled using the circulation it can be shown that they move with a velocity equal to the average of the fluid velocities on the right and left of $l_{\pm}(t)$ at $c_{\pm}(t)$. The interested reader is referred to Saffman (1992) for a detailed explanation. With these observations in mind,

application of the Plemelj formulae to equation (2.11), followed by the subsequent use of equations (2.2), (3.1), (3.2), and (3.3), eventually yields the ordinary differential equations

$$\dot{\Gamma}_{\pm}(t) = -\phi_{\pm}(c_{\pm}, t)(\mu(c_{\pm}, t) - \tau(t))\mathrm{e}^{\mathrm{i}(\theta(t)-\chi_{\pm}(t))}, \tag{3.14}$$

which govern the rate at which circulation is shed from the bound vortex sheet into the two free vortex sheets. In equation (3.14) the function $\mu(\zeta, t)$ takes the form

$$\mu(\zeta, t) = \mathrm{Im}\left\{\frac{\mathrm{e}^{\mathrm{i}\theta(t)}}{2\pi}\left[\int_0^{\Gamma_-(t)} \frac{\mathrm{d}\Lambda}{(\zeta_-(\Lambda, t) - \zeta)} - \int_0^{\Gamma_+(t)} \frac{\mathrm{d}\Lambda}{(\zeta_+(\Lambda, t) - \zeta)}\right]\right\}, \tag{3.15}$$

and is the tangential component of the average of the fluid velocities on the right and left of $l_{=}(t)$ at ζ. We also note that $\tau(t) = \mathrm{Re}\{\dot{c}(t)\,\mathrm{e}^{-\mathrm{i}\theta(t)}\}$ is the tangential component of the velocity of the plate. Therefore, the quantity $\mu(\zeta, t) - \tau(t)$ measures the average slip between the plate and the fluid. Expression (3.14) is in fact equivalent to that given by Prandtl & Tietjens (1934, p. 218).

3.2. *Removing the logarithmic singularities in* $\Phi(z, t)$

Having removed the inverse square-root singularities in $\Phi(z, t)$ through the introduction of the constraints (3.13), or the equivalent ordinary differential equations (3.14), we are next faced with the task of removing any remaining singularities in $\Phi(z, t)$. Since the vortex sheet strengths $\phi_{=}(\zeta, t)$ and $\phi_{\pm}(\zeta, t)$ are now bounded functions tending to well-defined limits as $\zeta \to c_{\pm}(t)$, the results stated in Appendix B show that, in general, $\Phi(z, t)$ is still expected to have logarithmic singularities at $z = c_{\pm}(t)$. Furthermore, consideration of the original definition of $\Phi(z, t)$, given in equation (2.3), shows that the boundary integrals over $l_{-}(t)$ and $l_{=}(t)$ will each contribute to the logarithmic singularity at $z = c_{-}(t)$ and the boundary integrals over $l_{=}(t)$ and $l_{+}(t)$ will each contribute to the logarithmic singularity at $z = c_{+}(t)$. With this in mind, we conclude that if the logarithmic singularities in $\Phi(z, t)$ are to be removed then the aforementioned contributions must be made to exactly cancel.

The conditions that ensure that these cancellations take place require that $\phi_{=}(c_{\pm}, t) = \phi_{\pm}(c_{\pm}, t)$ and can be derived by applying the results stated in Appendix B to equation (2.3). Subsequent use of equations (2.6), (3.7), and (3.10), to show that

$$\phi_{=}(c_{\pm}, t) = \phi_{\pm}(c_{\pm}, t)\mathrm{Re}\{\mathrm{e}^{\mathrm{i}\chi_{\pm}(t)}\}\,\mathrm{e}^{-\mathrm{i}\chi_{\pm}(t)}, \tag{3.16}$$

then allows us to deduce that the logarithmic singularities in $\Phi(z, t)$ are effectively removed if

$$\chi_{\pm}(t) = 0. \tag{3.17}$$

Considering the original definition of $\chi_{\pm}(t)$, as the angle between the plate and the tangent to $l_{\pm}(t)$ at $c_{\pm}(t)$, it is therefore clear that the free vortex sheets must separate tangentially if the logarithmic singularities in $\Phi(z, t)$ are to be removed. It is interesting to note that the condition that sets $\chi_{\pm}(t)$ equal to zero also allows the possibility that $\chi_{\pm}(t) = \pi$, which would result in the formation of a cusp in $l(t)$ at $c_{\pm}(t)$. However, this possibility is disregarded as unphysical.

3.3. *The time evolution of* $\Phi(z, t)$

Having ensured that $\Phi(z, t)$ satisfies all the required boundary conditions, we now move on to consider the question of how $\Phi(z, t)$ evolves in time. We begin by returning to equation (2.3) and note that $\Phi(z, t)$ depends only on the positions and strengths of the vortex sheets $l_{-}(t)$, $l_{=}(t)$, and $l_{+}(t)$. As a result, the problem reduces to that of

determining how these vortex sheets evolve in time. In fact, we need only consider the evolution of $l_{\pm}(t)$, since once their position and strength are known the position and strength of $l_{=}(t)$ can be deduced.

Fortunately, the problem of determining the time evolution of a free vortex sheet has already been considered by Birkhoff (1962) and Rott (1956) who solved the problem using a particularly elegant Lagrangian formulation. In this formulation the boundary condition which states that the pressure must be continuous across the vortex sheet is satisfied automatically. Furthermore, the formulation uses the circulation to label Lagrangian points on the sheet and these points are then shown to move with a velocity equal to the average of the fluid velocities on the right and left of the sheet. Application of these ideas to the problem under consideration yields the differential equations

$$\frac{\partial \overline{\zeta}_{\pm}}{\partial t}(\Gamma, t) = \frac{1}{2\pi \mathrm{i}} \left[\int_0^{\Gamma_-(t)} \frac{\mathrm{d}\Lambda}{(\zeta_-(\Lambda, t) - \zeta_{\pm}(\Gamma, t))} + \int_{l_{=}(t)} \frac{\phi_{=}(\lambda, t)\,\mathrm{d}\lambda}{(\lambda - \zeta_{\pm}(\Gamma, t))} - \int_0^{\Gamma_+(t)} \frac{\mathrm{d}\Lambda}{(\zeta_+(\Lambda, t) - \zeta_{\pm}(\Gamma, t))} \right] \tag{3.18}$$

which govern the time evolution of the free vortex sheets $l_{\pm}(t)$. Again, the free vortex sheets have been parameterized using the circulation $\Gamma(\zeta, t)$ and an overbar has been used to denote complex conjugation. Finally, we note that

$$\phi_{\pm}(c_{\pm}, t) = \left[\frac{\partial \zeta_{\pm}}{\partial \Gamma}(\Gamma_{\pm}(t), t) \right]^{-1}, \tag{3.19}$$

and equations (3.7)–(3.19) then form a closed system of first-order ordinary differential equations for the unknowns $\phi_{=}(\zeta, t)$, $\zeta_{\pm}(\Gamma, t)$, and $\Gamma_{\pm}(t)$. As such, equations (3.7)–(3.19) can be integrated forward in time, given the motion of the plate and appropriate initial conditions. Once $\phi_{=}(\zeta, t)$, $\zeta_{\pm}(\Gamma, t)$, and $\Gamma_{\pm}(t)$ have been determined, the velocity field in the fluid surrounding the plate can be reconstructed using equation (2.11).

3.4. *The force and torque on the plate*

At this point all that remains is to calculate the forces on the plate. As there is no viscosity in the problem, the only forces acting on the plate are normal pressure forces and these act with a magnitude proportional to the pressure difference across the plate, denoted $[p](\zeta, t) = p_{=}^{+}(\zeta, t) - p_{=}^{-}(\zeta, t)$. Consideration of the definition for the rate of change of circulation at a point fixed in the plate leads, after use of the non-dimensional Euler equations and a suitable change of frame, to an expression for $[p](\zeta, t)$ of the form

$$[p](\zeta, t) = -\frac{\mathrm{d}\Gamma}{\mathrm{d}t}(\zeta, t) - \phi_{=}(\zeta, t)(\mu(\zeta, t) - \tau(t))\,\mathrm{e}^{\mathrm{i}\theta(t)}, \tag{3.20}$$

where the full time derivative represents differentiation with respect to time while holding the arclength $s(\zeta, t)$ fixed. The pressure difference across the free vortex sheets is of course zero by construction and equation (3.20) therefore ensures the continuity of $[p](\zeta, t)$ by setting

$$[p](c_{\pm}, t) = 0. \tag{3.21}$$

The result (3.21) can be verified using equations (2.9), (3.7), (3.10), (3.14), and (3.17) in equation (3.20) with $\zeta = c_{\pm}(t)$. Having found $[p](\zeta, t)$, it is then possible to express the total normal force on the plate, denoted $\mathbb{F}(t)$, and the total torque on the plate, denoted $\mathbb{T}(t)$, as

$$\mathbb{F}(t) = -\mathrm{e}^{-\mathrm{i}\theta(t)} \int_{l_{=}(t)} [p](\lambda, t)\, \mathrm{d}\lambda, \tag{3.22}$$

$$\mathbb{T}(t) = -\mathrm{e}^{-2\mathrm{i}\theta(t)} \int_{l_{=}(t)} (\lambda - c)[p](\lambda, t)\, \mathrm{d}\lambda, \tag{3.23}$$

and this completes our description of the flow.

3.5. *An alternative formulation using Chebyshev series*

Before moving on to consider the numerical solution of equations (3.7)–(3.23) it is enlightening, both from a physical and numerical perspective, to re-derive equations (3.7)–(3.23) from a different starting point. We begin by rewriting the real part of equation (3.6) and the whole of equation (3.15) in the form of the Chebyshev series expansions:

$$\mathrm{Re}\{\psi(\zeta, t)\} = \sum_{n=0}^{\infty} \alpha_n(t) T_n(s(\zeta, t)), \tag{3.24}$$

$$\mu(\zeta, t) = \sum_{n=0}^{\infty} \beta_n(t) T_n(s(\zeta, t)), \tag{3.25}$$

where $T_n(s)$ denotes the nth-order Chebyshev polynomial of the first kind and the real coefficients $\alpha_n(t)$ and $\beta_n(t)$ can be expressed explicitly in terms of $\mathrm{Re}\{\psi(\zeta, t)\}$ and $\mu(\zeta, t)$ using the orthogonality of the Chebyshev polynomials. Using the expansions (3.24) and (3.25) as our starting point, it is then possible to repeat the calculation that lead to equations (3.7)–(3.23) and we find that $\phi_{=}(\zeta, t)$ again takes the form (3.7). However, this time the functions $A(t)$, $B(t)$, and $C(\zeta, t)$ are rewritten in the form

$$A(t) = \Gamma_{+}(t) - \Gamma_{-}(t) - \gamma_{+}(c_{+}, t) - \gamma_{-}(c_{-}, t) + \pi(\dot{\theta}(t) - \alpha_1(t)), \tag{3.26}$$

$$B(t) = \log(2)(\gamma_{-}(c_{-}, t) - \gamma_{+}(c_{+}, t)) + 2\pi(\eta(t) - \alpha_0(t)), \tag{3.27}$$

and

$$C(\zeta, t) = 2\pi\dot{\theta}(t) - 2\pi \sum_{n=1}^{\infty} \alpha_n(t) U_{n-1}(s(\zeta, t)), \tag{3.28}$$

where $U_{n-1}(s)$ denotes the $(n-1)$th-order Chebyshev polynomial of the second kind.

The reader should note that equations (3.26)–(3.28) are only valid under the assumption that $\chi_{\pm}(t) = 0$, as was shown to be the case in equation (3.17). Again, the unsteady Kutta condition states that the inverse square-root singularities in $\phi_{=}(\zeta, t)$ must be removed by satisfying the additional constraints $A(t) \pm B(t) = 0$, which now take the form

$$\Gamma_{+}(t) - \Gamma_{-}(t) - k_{\pm}\gamma_{+}(c_{+}, t) - k_{\mp}\gamma_{-}(c_{-}, t) + \pi(\dot{\theta}(t) - \alpha_1(t)) \pm 2\pi(\eta(t) - \alpha_0(t)) = 0, \tag{3.29}$$

where $k_{\pm} = 1 \pm \log(2)$. We note that the coefficients $\alpha_0(t)$ and $\alpha_1(t)$ depend implicitly on $\Gamma_{\pm}(t)$, through equations (3.6) and (3.24), and so no explicit solution for $\Gamma_{\pm}(t)$ is forthcoming. However, the constraints (3.29) can be solved simultaneously for

$\Gamma_{\pm}(t)$, in principle. Once the constraints (3.29) have been satisfied it is possible, using equations (3.6), (3.7), and (3.28) to rewrite equation (3.18) in the form

$$\frac{\partial \overline{\zeta}_{\pm}}{\partial t}(\Gamma, t) = -\mathrm{i}\,\mathrm{e}^{-\mathrm{i}\theta(t)}\left[\frac{1}{\pi}(\Gamma_{+}(t) - \Gamma_{-}(t))\upsilon_1(\zeta_{\pm}(\Gamma, t), t) + \gamma_{+}(c_{+}, t)\upsilon_{+}(\zeta_{\pm}(\Gamma, t), t) + \gamma_{-}(c_{-}, t)\upsilon_{-}(\zeta_{\pm}(\Gamma, t), t) + \psi(\zeta_{\pm}(\Gamma, t), t) + \sum_{n=2}^{\infty}\alpha_n(t)\upsilon_n(\zeta_{\pm}(\Gamma, t), t)\right], \tag{3.30}$$

where

$$\upsilon_{\pm}(\zeta, t) = \frac{1}{2\pi}\int_{l_{=}(t)}\frac{a_{\pm}(s(\lambda, t))}{(\lambda - \zeta)}\,\mathrm{d}\lambda \mp \frac{1}{2\pi}\log(\zeta - c_{\pm}) - \frac{1}{\pi}\upsilon_1(\zeta, t), \tag{3.31}$$

$$\upsilon_n(\zeta, t) = -(\sigma(\zeta, t) - \sqrt{\sigma(\zeta, t) + 1}\sqrt{\sigma(\zeta, t) - 1})^n, \tag{3.32}$$

for $n = 1, 2, \ldots,$ and $\sigma(\zeta, t) = (\zeta - c)\,\mathrm{e}^{-\mathrm{i}\theta(t)}$. From a numerical perspective equation (3.30) is preferred over equation (3.18) since $\upsilon_{\pm}(\zeta, t)$ and $\upsilon_n(\zeta, t)$ for $n = 1, 2, \ldots$ are all well-defined bounded functions of ζ. Moreover, it is possible to push the use of the Chebyshev expansions (3.24) and (3.25) even further by deriving alternative expressions for $\Gamma(\zeta, t)$, $\mathbb{F}(t)$ and $\mathbb{T}(t)$.

We begin by substituting the Chebyshev expansion for $\phi_{=}(\zeta, t)$ into equation (2.7) and continue by evaluating the resulting integrals over $l_{=}(\zeta, t)$ exactly using the special properties of the Chebyshev polynomials. After some work we obtain $\Gamma(\zeta, t)$ in the form

$$\Gamma(\zeta, t) = \Gamma_{+}(t)b_{+}(s) + \Gamma_{-}(t)b_{-}(s) + \gamma_{+}(c_{+}, t)d_{+}(s) + \gamma_{-}(c_{-}, t)d_{-}(s) + e(s, t), \tag{3.33}$$

where

$$b_{\pm}(s) = a_{\pm}(s) \pm \frac{1}{\pi}s\sqrt{1 + s}\sqrt{1 - s}, \tag{3.34}$$

$$d_{\pm}(s) = \mp(1 \mp s)\left[a_{\pm}(s) - \frac{1}{\pi}\sqrt{1 + s}\sqrt{1 - s}\right], \tag{3.35}$$

$$e(s, t) = \sqrt{1 + s}\sqrt{1 - s}\sum_{n=2}^{\infty}\alpha_n(t)\left[\frac{U_n(s)}{(n + 1)} - \frac{U_{n-2}(s)}{(n - 1)}\right]. \tag{3.36}$$

In (3.34)–(3.36) the explicit dependence of $s(\zeta, t)$ on ζ and t has been omitted for clarity. Having found $\Gamma(\zeta, t)$ in the form (3.33) it is then possible to construct a Chebyshev expansion for $[p](\zeta, t)$ by combining the Chebyshev expansions for $\Gamma(\zeta, t)$, $\phi_{=}(\zeta, t)$, and $\mu(\zeta, t)$ according to equation (3.20). Explicit expressions for $\mathbb{F}(t)$ and $\mathbb{T}(t)$ can then be obtained by using the resulting expansion in equations (3.22) and (3.23) followed by the exact evaluation of the remaining integrals over $l_{=}(t)$. After a significant amount of algebra we obtain $\mathbb{F}(t)$ and $\mathbb{T}(t)$ in the forms

$$\mathbb{F}(t) = \mathbb{F}_s(t) + \mathbb{F}_u(t) + \mathbb{F}_w(t), \tag{3.37}$$

$$\mathbb{T}(t) = \mathbb{T}_s(t) + \mathbb{T}_u(t) + \mathbb{T}_w(t), \tag{3.38}$$

where

$$\mathbb{F}_s(t) = (\Gamma_{+}(t) - \Gamma_{-}(t))\big(\beta_0(t) - \tfrac{1}{2}\beta_2(t) - \tau(t)\big) + \gamma_{+}(c_{+}, t)g_{+}(t) + \gamma_{-}(c_{-}, t)g_{-}(t),$$

$$\mathbb{T}_s(t) = \tfrac{1}{4}(\Gamma_{+}(t) - \Gamma_{-}(t))(\beta_1(t) - \beta_3(t)) + \gamma_{+}(c_{+}, t)h_{+}(t) + \gamma_{-}(c_{-}, t)h_{-}(t)$$

are the steady components of the normal force and torque,

$$\mathbb{F}_u(t) = \dot{\Gamma}_+(t) + \dot{\Gamma}_-(t) - \tfrac{1}{4}(\dot{\gamma}_+(c_+, t) - \dot{\gamma}_-(c_-, t)) - \tfrac{1}{2}\pi\dot{\alpha}_2(t),$$
$$\mathbb{T}_u(t) = \tfrac{3}{8}(\dot{\Gamma}_+(t) - \dot{\Gamma}_-(t)) - \tfrac{1}{24}(\dot{\gamma}_+(c_+, t) + \dot{\gamma}_-(c_-, t)) - \tfrac{1}{8}\pi\dot{\alpha}_3(t)$$

are the unsteady components of the normal force and torque, and

$$\mathbb{F}_w(t) = \frac{\pi}{2}\sum_{n=2}^{\infty}\alpha_n(t)(\beta_{n-1}(t) - \beta_{n+1}(t)),$$

$$\mathbb{T}_w(t) = \frac{\pi}{4}\alpha_2(t)(\beta_0(t) - 2\tau(t)) + \frac{\pi}{4}\sum_{n=2}^{\infty}\alpha_n(t)(\beta_{n-2}(t) - \beta_{n+2}(t))$$

are the components of the normal force and torque that are induced by the presence of the circulation in the wake. To complete the definitions of $\mathbb{F}_s(t)$ and $\mathbb{T}_s(t)$ it is necessary to note that

$$g_\pm(t) = \tfrac{1}{2}\beta_2(t) \pm \tfrac{1}{4}\beta_1(t) - \sum_{m=2}^{\infty}\frac{(\pm 1)^m}{(m+1)(m-1)}\beta_m(t),$$

$$h_\pm(t) = \tfrac{1}{4}\beta_3(t) \pm \tfrac{1}{16}\beta_2(t) + \tfrac{1}{12}\beta_1(t) \pm \tfrac{1}{4}\beta_0(t) \mp \tfrac{1}{4}\tau(t) - \sum_{m=3}^{\infty}\frac{(\pm 1)^{m+1}}{(m+2)(m-2)}\beta_m(t).$$

At first glance these two equations appear complicated and rather cumbersome. However, on closer examination the steady and unsteady components are found to be relatively simple. In any event equations (3.37) and (3.38) are included in full since they are likely to provide insight into the high-lift mechanisms of unsteady aerodynamics. Having re-derived the governing equations from a different starting point we now move on to consider how the flows under investigation are started-up from rest.

4. Asymptotic small-time solution

In general, the motion under consideration is always started-up from rest and so the question of how the free vortex sheets $l_\pm(t)$ come into existence is an important one. We can answer this question by constructing a small-time asymptotic solution to the system of equations (3.7)–(3.19). Just after start-up from rest, the theoretical and experimental work of Moore (1974, 1975), Pullin (1978), and Pullin & Perry (1980) suggests that the flow solution consists of two small starting vortices, one at each of the plate's edges, which take the form of two infinite spiral vortex sheets. For small enough times $t > 0$, these spiral vortex sheets are expected to have approximately self-similar structure in time due to the absence of a typical length scale in the regions surrounding the edges of the plate. With this in mind it is possible to show, using scaling arguments, that if the initial motion of the plate is consistent with the following small-time asymptotic expansions for $c(t)$ and $\theta(t)$:

$$c(t) \sim c_0 + \alpha_0 t^{m+1}\mathrm{e}^{\mathrm{i}\vartheta_0} + \cdots, \tag{4.1}$$
$$\theta(t) \sim \theta_0 + \beta_0 t^{m+1} + \cdots, \tag{4.2}$$

then the system of equations (3.7)–(3.19) admits asymptotically self-similar solutions of the form

$$\zeta_\pm(\Gamma, t) \sim c_\pm(t) \pm |\delta_\pm|^{2/3} t^{2(m+1)/3}\omega_\pm(\tau_\pm)\,\mathrm{e}^{\mathrm{i}\theta(t)} + \cdots, \tag{4.3}$$
$$\Gamma_\pm(t) \sim J_\pm|\delta_\pm|^{4/3} t^{(4m+1)/3} + \cdots, \tag{4.4}$$

where the similarity variables $\tau_{\pm}(\Gamma, t)$ are defined as

$$\tau_{\pm}(\Gamma, t) = 1 - \Gamma J_{\pm}^{-1} |\delta_{\pm}|^{-4/3} t^{-(4m+1)/3}. \tag{4.5}$$

The functions $\omega_{\pm}(\tau_{\pm})$ and the constants $\delta_{\pm}$ and $J_{\pm}$ are to be determined. Subsequent substitution of the asymptotic expansions (4.1)–(4.4) into equation (3.18), followed by the series expansion of the result in powers of t using equations (3.7) and (3.10), yields the complex integro-differential equations

$$p\overline{\omega}_{\pm}(\tau_{\pm}) + q(1-\tau_{\pm})\overline{\omega}'_{\pm}(\tau_{\pm}) = \mp \frac{J_{\pm}}{2\pi \mathrm{i}} \left[\int_0^1 \frac{\mathrm{d}\tau}{\omega_{\pm}(\tau) - \omega_{\pm}(\tau_{\pm})} + \int_{-\infty}^0 \frac{\sqrt{-\xi} F_{\pm}(\xi)}{(\xi - \omega_{\pm}(\tau_{\pm}))} \, \mathrm{d}\xi \right], \tag{4.6}$$

which must be solved for $\omega_{\pm}(\tau_{\pm})$ and $J_{\pm}$. In (4.6) $p = 2(m+1)/3$, $q = (4m+1)/3$,

$$F_{\pm}(\xi) = \frac{1}{\pi} \int_0^1 \mathrm{Re} \left\{ \frac{1}{\sqrt{\omega_{\pm}(\tau)}(\omega_{\pm}(\tau) - \xi)} \right\} \mathrm{d}\tau, \tag{4.7}$$

and terms of higher order than $O(t^{(2m-1)/3})$ have been discarded. The reader will note that equations (4.6) are un-coupled and therefore our initial assumption, that the starting vortex at one edge is not influenced by its counterpart at the other edge, is justified as a first approximation.

Next, we derive expressions for the unknown constants $\delta_{\pm}$ and $J_{\pm}$. To do this the constraints (3.13) are preferred over the ordinary differential equations (3.14) since, in the current self-similar context, no initial conditions are available. With this in mind, substitution of the asymptotic expansions (4.1)–(4.4) into equations (3.13), followed by the series expansion of the result in powers of t, yields the unknown constants $\delta_{\pm}$ and $J_{\pm}$ in the form

$$\delta_{\pm} = \alpha_0 \sin(\vartheta_0 - \theta_0) \pm \frac{\beta_0}{2}, \tag{4.8}$$

$$J_{\pm} = -\sqrt{2}\pi(m+1)\mathrm{sgn}\delta_{\pm} \left[\int_0^1 \mathrm{Re} \left\{ \frac{1}{\sqrt{\omega_{\pm}(\tau)}} \right\} \mathrm{d}\tau \right]^{-1}, \tag{4.9}$$

where terms of higher order than $O(t^m)$ have been discarded. Equations (4.6)–(4.9) can then be solved for $\omega_{\pm}(\tau_{\pm})$ and $J_{\pm}$ numerically subject to the boundary conditions $\omega_{\pm}(0) = 0$ and $\mathrm{Im}\{\omega'_{\pm}(0)\} = 0$, which ensure that the spiral vortex sheets join to the edges of the plate and separate tangentially. This was done for a range of values of m using an approach not unlike that used by Pullin (1978) and the solutions for $\omega_{\pm}(\tau_{\pm})$ and $J_{\pm}$ were found to be in excellent agreement with those of Pullin (1978).

4.1. *A simple small-time point-vortex solution*

In terms of the current study, it is more useful to consider the case where the two infinite spiral vortex sheets are replaced by two point vortices whose circulations and positions, denoted by $\Gamma_{\pm}(t)$ and $\zeta_{\pm}(t)$ respectively, are allowed to vary self-similarly in time according to the small-time asymptotic expansions

$$\zeta_{\pm}(t) \sim c_{\pm}(t) \pm |\delta_{\pm}|^{2/3} t^{2(m+1)/3} \Omega_{\pm} \mathrm{e}^{\mathrm{i}\theta(t)} + \cdots, \tag{4.10}$$

$$\Gamma_{\pm}(t) \sim K_{\pm} |\delta_{\pm}|^{4/3} t^{(4m+1)/3} + \cdots. \tag{4.11}$$

The reader is referred to Cortelezzi & Leonard (1993) for a previous derivation of such a solution using a conformal mapping technique. In this case equations (4.6),

(4.7), and (4.9) simplify somewhat and combine to yield two un-coupled integral equations of the form

$$\overline{\Omega}_{\pm} \mp \frac{3\,\mathrm{sgn}\delta_{\pm}}{2\sqrt{2}\pi\mathrm{i}}\left[\mathrm{Re}\left\{\frac{1}{\sqrt{\Omega_{\pm}}}\right\}\right]^{-1}\int_{-\infty}^{0}\frac{\sqrt{-\xi}}{(\xi-\Omega_{\pm})}\mathrm{Re}\left\{\frac{1}{\sqrt{\Omega_{\pm}}(\Omega_{\pm}-\xi)}\right\}\mathrm{d}\xi = 0, \tag{4.12}$$

which can be solved exactly, assuming that $\Omega_{\pm}$ is purely imaginary. The quantity $K_{\pm}$ can then be expressed in terms of $\Omega_{\pm}$ using a simplified version of equation (4.9). In fact, $\Omega_{\pm}$ and $K_{\pm}$ must take the values

$$\Omega_{\pm} = \mp i(3/8)^{2/3}\,\mathrm{sgn}\delta_{\pm}, \tag{4.13}$$

$$K_{\pm} = -2\pi(3/8)^{1/3}(m+1)\,\mathrm{sgn}\delta_{\pm}, \tag{4.14}$$

where the constants $\delta_{\pm}$ are defined in equation (4.8). The simplicity of this self-similar point-vortex solution makes it an ideal candidate for use as an initial condition in the following numerical treatment of the full system of equations.

5. Numerical solution

Having derived the ordinary differential equations that govern the evolution of $\Phi(z,t)$ and explored the small-time solution of those equations asymptotically, we are now in a position to consider the general numerical solution of equations (3.7)–(3.19). Unfortunately, we are faced with a seemingly insurmountable problem at the outset since equations (3.7)–(3.19) are ill-posed. In other words, if we were to evolve a numerical approximation to the solution of equations (3.7)–(3.19) according to equation (3.18) then the errors inherent in that numerical approximation would grow in time, eventually obscuring the true solution. For a detailed study of this phenomenon see Krasny (1986*a*). Moreover, equations (3.7)–(3.19) admit solutions with finite time singularities, akin to those discovered by Moore (1979) and studied by Krasny (1986*a*), and so could only be integrated up to some critical time in any event. As a result, further progress seems unlikely.

However, the work of Chorin & Bernard (1973) and later Krasny (1986*a*, 1987), and Nitsche & Krasny (1994) shows that progress is possible if we consider the solution of a modified system of ordinary differential equations, which converge to equations (3.7)–(3.19) in some limit. A good candidate for such a system of differential equations can be derived by considering the time evolution of the complex-conjugate velocity field

$$\Phi(z,t) = \frac{1}{2\pi\mathrm{i}}\left[\int_{0}^{\Gamma_{-}(t)} K_{\delta}(\zeta_{-}(\Lambda,t)-z)\,\mathrm{d}\Lambda + \int_{l_{=}(t)}\frac{\phi_{=}(\lambda,t)}{(\lambda-z)}\,\mathrm{d}\lambda - \int_{0}^{\Gamma_{+}(t)} K_{\delta}(\zeta_{+}(\Lambda,t)-z)\,\mathrm{d}\Lambda\right], \tag{5.1}$$

where the kernel $K_{\delta}(z)$ takes the desingularized form

$$K_{\delta}(z) = \frac{|z|^2}{(|z|^2+\delta^2)}\frac{1}{z}, \tag{5.2}$$

and is sometimes referred to as the vortex-blob kernel. Since $K_{\delta}(z)$ approaches the Cauchy kernel as $\delta \to 0$ it is hoped that the solution of the resulting system of ordinary differential equations will converge to the true solution as $\delta \to 0$, although this conjecture has not been rigorously proven as yet. It is also hoped that the

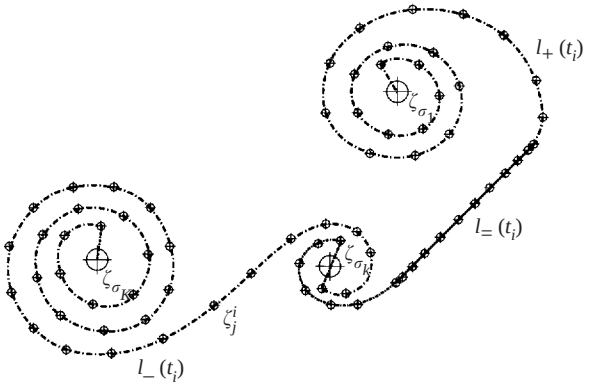

FIGURE 3. A diagram of the discretized flat plate $l_=(t_i)$, its discretized trailing vortex sheets $l_\pm(t_i)$, the Lagrangian points ζ_j^i, and the spiral centres $\zeta_{\sigma_1}^i$, $\zeta_{\sigma_k}^i$, and $\zeta_{\sigma_K}^i$ at some time $t_i > 0$.

resulting system of ordinary differential equations will be well-posed for $\delta > 0$ since the desingularized kernel $K_\delta(z)$ suppresses the Kelvin–Helmholtz instability, inherent in equation (3.18), at wavelengths below a critical wavelength of order δ. Of course, $\Phi(z, t)$ no longer represents a solution to the governing Euler equations for $\delta > 0$ and the author urges the reader to keep this fact in mind throughout the remainder of the paper. It should also be noted that the unknowns $\Phi(z, t)$, $\phi_=(\zeta, t)$, $\zeta_\pm(\Gamma, t)$, and $\Gamma_\pm(t)$ are now parametrically dependent on δ, although this dependence has been omitted in equation (5.1) for clarity.

In order to derive the modified system of differential equations we perform an updated version of the calculation outlined in § 3. As in the latter part of § 3 we again employ the extensive use of Chebyshev polynomial expansions in order that all integrations over $l_=(t)$ can be performed exactly. This manoeuvre is essential in the current context since the non-analytic nature of the modified kernel $K_\delta(z)$ now prevents us from using techniques such as complex contour integration to evaluate these integrals. The modified calculation again leads to the results presented in equations (3.26)–(3.38) with the following exceptions. First, the definition of $\psi(\zeta, t)$, given in equation (3.6), is updated to become

$$\psi(\zeta, t) = \frac{e^{i\theta(t)}}{2\pi}\left[\int_0^{\Gamma_-(t)} K_\delta(\zeta_-(\Lambda, t) - \zeta)\,d\Lambda \int_0^{\Gamma_+(t)} K_\delta(\zeta_+(\Lambda, t) - \zeta)\,d\Lambda\right]. \tag{5.3}$$

Second, the definition of $\mu(\zeta, t)$, given in equation (3.15), is updated to become $\mu(\zeta, t) = \mathrm{Im}\{\psi(\zeta, t)\}$. And third, all the terms that contain the constants $\gamma_\pm(c_\pm, t)$ are effectively set to zero. Unfortunately, these seemingly innocuous changes have some rather undesirable consequences, which include the introduction of jump discontinuities into the vortex sheet strength and the pressure difference at $\zeta = c_\pm(t)$. However, these discontinuities are not altogether unexpected given the discontinuous nature of the effective kernel in equation (5.1). Having described the modifications to equations (3.26)–(3.38) that are required if $\delta > 0$, we now turn to the specifics of how the modified system of ordinary differential equations is to be solved numerically.

To begin, we partition the time interval over which the solution is required into I sub-intervals separated by the discrete times t_i, where $i = 0, \ldots, I$ and $t_0 = 0$. At time t_i we discretize the vortex sheet $l(t_i)$ using J Lagrangian points and denote their positions using the complex numbers ζ_j^i, where $j = 1, \ldots, J$, see figure 3. The integer

j is referred to as the Lagrangian index of the point ζ_j^i. To avoid ambiguity we define ζ_1^i as the free end of $l_+(t_i)$ and ζ_J^i as the free end of $l_-(t_i)$. Additionally, we use the integers p and q to denote the Lagrangian indices of the points $c_+(t_i)$ and $c_-(t_i)$ respectively. Finally, we denote the circulation at the points ζ_j^i using the real numbers Γ_j^i for $j=1,\ldots,J$ and therefore require that $\Gamma_p^i=\Gamma_+(t_i)$, $\Gamma_q^i=\Gamma_-(t_i)$, and $\Gamma_1^i=\Gamma_J^i=0$.

Experience suggests that during the evolution of the flow certain portions of $l(t)$ will roll up into tightly wound spirals. In this scheme, we choose to faithfully represent only the outermost turns of these spirals and replace their inner turns with K isolated point vortices, one at each of the spiral centres. The Lagrangian index of the kth spiral centre is denoted σ_k, where $k=1,\ldots,K$, and as a result the position and circulation of the kth spiral centre are denoted $\zeta_{\sigma_k}^i$ and $\Gamma_{\sigma_k}^i$ respectively. We note that there are always at least two such spiral centres in the flow and therefore use the convention that $\sigma_1=1$ and $\sigma_K=J$. At this point we also note that the times t_i can either be prescribed or chosen dynamically and that additional Lagrangian points may need to be inserted into the calculation from time to time in order to cope with the appearance of unexpected complexity in $l(t)$.

5.1. *The time-marching algorithm*

Having discretized the vortex sheets we next consider how the position and strength of the vortex sheets will be updated from one time step to the next. We begin by assuming that ζ_j^i and Γ_j^i are known for $j=1,\ldots,p-1,q+1,\ldots,J$ and we define

$$\zeta_j^i = c(t_i) + \cos(\pi(j-p)/(q-p))\mathrm{e}^{\mathrm{i}\theta(t_i)}, \tag{5.4}$$

for $j=p,\ldots,q$. Next we estimate Γ_p^i and Γ_q^i and our task then becomes that of finding approximate expressions for the unknowns ζ_j^{i+1} and Γ_j^{i+1} for $j=1,\ldots,p-1$, $q+1,\ldots,J$ in terms of the known quantities listed immediately above. To do this we must first find an accurate and efficient numerical method for evaluating the right-hand side of equation (3.30) at the points ζ_j^i for $j=1,\ldots,p-1,q+1,\ldots,J$.

Given that all the terms containing the constants $\gamma_\pm(c_\pm,t)$ have effectively been set to zero, the right-hand side of equation (3.30) now consists of just three terms and we begin by approximating the second of these, $\psi(\zeta_j^i,t)$, by

$$\psi_j^i = -\frac{\mathrm{e}^{\mathrm{i}\theta(t_i)}}{2\pi}\left[\sum_{\substack{k=1\\ \sigma_k\neq j}}^{K}\frac{w_{\sigma_k}}{(\zeta_{\sigma_k}^i-\zeta_j^i)} + \frac{1}{2}\sum_{m\notin\{\sigma_k:k=1,\ldots,K\}}^{J} w_m K_\delta(\zeta_m^i-\zeta_j^i)\right], \tag{5.5}$$

for $j=1,\ldots,J$. This approximation is derived by replacing the integrals in equation (5.3) with the discrete sums that result from the application of a simple trapezoidal quadrature rule and as a result the weights w_j^i take the form

$$w_j^i = \begin{cases} (\Gamma_{j+1}^i-\Gamma_j^i) & \text{for} \quad j\in\{\sigma_k+1:k=1,\ldots,K-1\}\cup\{q\}\cup\{\sigma_1\} \\ (\Gamma_{j+1}^i-\Gamma_{j-1}^i) & \text{for} \quad j\in\{\sigma_k+2,\ldots,\sigma_{k+1}-2:k=1,\ldots,K-1\}\backslash\{p,\ldots,q\} \\ 0 & \text{for} \quad j\in\{p+1,\ldots,q-1\} \\ (\Gamma_{j+1}^i-\Gamma_{j-1}^i) & \text{for} \quad j\in\{\sigma_k:k=2,\ldots,K-1\} \\ (\Gamma_j^i-\Gamma_{j-1}^i) & \text{for} \quad j\in\{\sigma_k-1:k=2,\ldots,K\}\cup\{p\}\cup\{\sigma_K\} \end{cases} \tag{5.6}$$

for $j=1,\ldots,J$.

The first term in equation (5.5) is a sum over the spiral centres ζ_{σ_k} and as such it approximates an integral over those portions of $l_{\pm}(t_i)$ that qualify as the inner turns of tightly wound spirals; a point-vortex approximation is used in these areas. The second term approximates the remaining portions of the integrals over $l_{\pm}(t_i)$ using a vortex-blob approximation. Both terms can be evaluated efficiently using fast summation techniques and the interested reader is referred to the work of Greengard & Rokhlin (1987) and Draghicescu & Draghicescu (1995) for a detailed account of the respective algorithms.

We next approximate the combination of the Chebyshev coefficients $\alpha_n(t_i) + i\beta_n(t_i)$ by

$$\alpha_n^i + \mathrm{i}\beta_n^i = \frac{k_n}{(q-p)} \left[\tfrac{1}{2}\psi_p^i + \sum_{m=p+1}^{q-1} \psi_j^i \cos(n\pi(m-p)/(q-p)) + \tfrac{1}{2}(-1)^n \psi_q^i \right], \quad (5.7)$$

for $n = 0, \ldots, q-p$, where $k_0 = 1$, $k_n = 2$ for $n = 1, \ldots, q-p-1$, and $k_{q-p} = 1$. Equation (5.7) is derived by requiring that a truncated version of the infinite sums in equations (3.24) and (3.25) interpolate the real and imaginary parts of ψ_j^i at the points ζ_j^i for $j = p, \ldots, q$. The resulting sum can be evaluated efficiently using a variant of the fast Fourier transform.

Having described an efficient way to calculate α_n^i and β_n^i for $n = 0, \ldots, q-p$ we continue by outlining a way to correct the estimated values of the unknown circulations Γ_p^i and Γ_q^i. We begin by rewriting the modified version of equation (3.29) in the discrete form

$$\Gamma_p^i - \Gamma_q^i + \pi\big(\dot{\theta}(t_i) - \alpha_1^i\big) \pm 2\pi\big(\eta(t_i) - \alpha_0^i\big) = 0, \quad (5.8)$$

and note that, in general, these constraints will not be satisfied in the first instance. Fortunately, it is always possible to satisfy them by adjusting the unknown circulations Γ_p^i and Γ_q^i and this is done using a one-step Newton–Raphson algorithm, which yields an explicit solution for Γ_p^i and Γ_q^i. The details of this solution are omitted, but we remind the reader that the values of ψ_j^i, α_n^i, and β_n^i for $j = 1, \ldots, J$ and $n = 0, \ldots, q-p$ must also be corrected and that this can also be done as part of the one-step Newton–Raphson algorithm.

Having explicitly determined the corrected values for ψ_j^i, α_n^i, β_n^i, and the unknown circulations Γ_p^i and Γ_q^i we are finally in a position to evaluate our approximation to the right-hand side of equation (3.30). We approximate the right-hand side of the modified version of equation (3.30) by

$$\frac{\partial \overline{\zeta}_j^i}{\partial t} = -\mathrm{i}e^{-\mathrm{i}\theta(t_i)} \left[\frac{1}{\pi}\big(\Gamma_p^i - \Gamma_q^i\big)\upsilon_1\big(\zeta_j^i, t_i\big) + \psi_j^i + \sum_{n=2}^{q-p} \alpha_n^i \upsilon_n\big(\zeta_j^i, t_i\big) \right], \quad (5.9)$$

for $j = 1, \ldots, p-1, q+1, \ldots, J$. Taken together, equations (5.4)–(5.9) then constitute an accurate and efficient method for evaluating the time rate of change of ζ_j^i for $j = 1, \ldots, p-1, q+1, \ldots, J$. As such they can be used as part of a Runge–Kutta algorithm to construct approximations to ζ_j^{i+1} for $j = 1, \ldots, p-1, q+1, \ldots, J$. The details of the Runge–Kutta algorithm are not included here. To conclude, expressions for the circulations Γ_j^{i+1} for $j = 1, \ldots, p-1, q+1, \ldots, J$ can be derived by noting that the circulation is a Lagrangian variable on the free vortex sheets and so we have

$$\Gamma_j^{i+1} = \Gamma_j^i, \quad (5.10)$$

for $j = 1, \ldots, p-1, q+1, \ldots, J$. Should the values of Γ_j^i be required for $j = p+1, \ldots, q-1$ they can be approximated using a discretized and truncated version of equation (3.33). Similarly $\mathbb{F}(t_i)$ and $\mathbb{T}(t_i)$ can be approximated using truncated versions of equations (3.37)–(3.39) where the terms containing $\gamma_\pm(c_\pm, t)$ have been set to zero. This completes the definition of the basic time marching algorithm.

In order to faithfully represent the continual shedding of vorticity from the edges of the plate new Lagrangian points are inserted into the calculation at the beginning of every time step. Since the boundedness of $\Phi(z, t)$ is assured these new Lagrangian points can be placed exactly at the edges $\zeta = c_\pm(t)$ without difficulty. In order to accurately represent the increasingly complicated shape of the free vortex sheets we use an adaptive point insertion algorithm. This algorithm automatically inserts new Lagrangian points into the calculation so that approximately straight portions of $l(t_i)$ are represented by a minimum of P points per unit length, so that approximately circular portions of $l(t_i)$ are represented by minimum of Q points per turn, and so that a number of such portions remain smoothly joined together. In practice this is achieved by inserting a new point between the points ζ_j^i and ζ_{j-1}^i if any of the inequalities

$$\left|\zeta_j^i - \zeta_{j-1}^i\right| \geqslant \frac{1}{P}, \tag{5.11}$$

or

$$\max\left\{\left|\operatorname{Im}\left\{\log\left(\frac{\zeta_j^i - \zeta_{j-1}^i}{\zeta_{j-1}^i - \zeta_{j-2}^i}\right)\right\}\right|, \left|\operatorname{Im}\left\{\log\left(\frac{\zeta_{j+1}^i - \zeta_j^i}{\zeta_j^i - \zeta_{j-1}^i}\right)\right\}\right|\right\} \geqslant \frac{2\pi}{Q}, \tag{5.12}$$

or

$$\max\left\{\frac{\left|\zeta_j^i - \zeta_{j-1}^i\right|}{\left|\zeta_{j-1}^i - \zeta_{j-2}^i\right|}, \frac{\left|\zeta_j^i - \zeta_{j-1}^i\right|}{\left|\zeta_{j+1}^i - \zeta_j^i\right|}\right\} \geqslant R, \tag{5.13}$$

are satisfied. The position at which to insert the new point is determined using midpoint local cubic interpolation that uses the polygonal arclength as the underlying parametric variable. A similar procedure is used to determine the circulation of the new point. Of course, greater care must be taken when inserting points in the vicinity of the spiral centres or the edges of the plate, but the details are not discussed here.

In order to limit the number of turns that are faithfully represented in the vicinity of each spiral centre certain Lagrangian points are deleted from the calculation at the beginning of each time step. In practice, a point ζ_j^i is deleted if

$$\left|\theta_j^i\right| > 2\pi T, \tag{5.14}$$

where θ_j^i is the cumulative tangent angle of $l(t_i)$ at ζ_j^i and T is the number of turns required. The circulation in the deleted part of the vortex sheet is automatically added to the strength of the point vortex at the nearest spiral centre.

We now move on to discuss how the numerical solution is initialized at time $t_1 > 0$. As we have seen in §4 the true solution consists of two small starting vortices, one at each of the plate's edges, which take the form of two infinite spiral vortex sheets. However, as mentioned in §4, we choose to represent these structures using two point vortices whose positions and strengths are determined using an asymptotically self-similar theory. In practice, we begin by setting the constants c_0, θ_0, ϑ_0, α_0, β_0, m, $\delta_\pm$, $\Omega_\pm$, and $K_\pm$ in a way consistent with their definitions in §4. We then continue by setting $p = 2$, $q = J-1$, $K = 2$, $\sigma_1 = 1$, and $\sigma_K = J$ for given initial J. The solution is

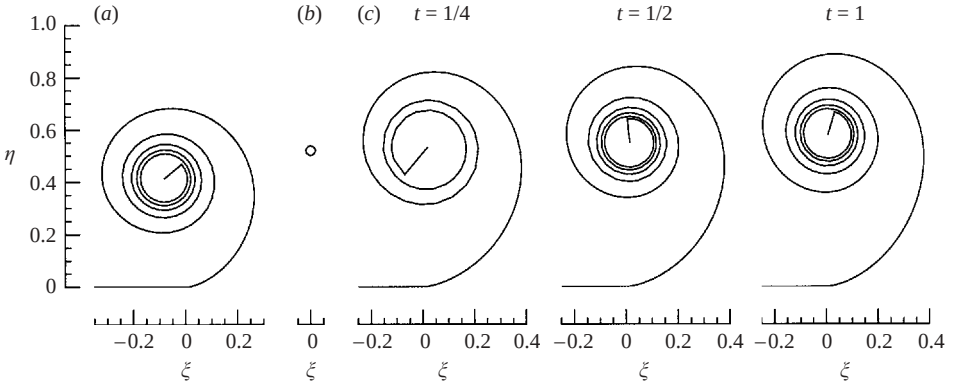

FIGURE 4. The spiral vortex formed by the impulsively started steady translation of a flat plate at constant angle of attack with $c(t)=t$ and $\theta(t)=\pi/2$. A comparison between (a) the small-time spiral-vortex solution for $\omega_{\pm}(\tau_{\pm})$, (b) the small-time point-vortex solution for $\Omega_{\pm}$, and (c) the numerical solution for $\zeta_{\pm}(\Gamma,t)$ at times $t=1/4$, $t=1/2$, and $t=1$ ($\delta=0.2$).

then initialized by setting

$$\Gamma_1^1 = 0, \tag{5.15}$$

$$\Gamma_J^1 = 0, \tag{5.16}$$

$$\zeta_1^1 = c_+(t_1) + |\delta_+|^{2/3} t_1^{2(m+1)/3} \Omega_+ \mathrm{e}^{\mathrm{i}\theta(t_1)}, \tag{5.17}$$

$$\zeta_J^1 = c_-(t_1) \pm |\delta_-|^{2/3} t_1^{2(m+1)/3} \Omega_- \mathrm{e}^{\mathrm{i}\theta(t_1)}, \tag{5.18}$$

and initial estimates for the unknown circulations Γ_p^1 and Γ_q^1 are made according to the formulae

$$\Gamma_p^1 = K_+ |\delta_+|^{4/3} t_1^{(4m+1)/3}, \tag{5.19}$$

$$\Gamma_q^1 = K_- |\delta_-|^{4/3} t_1^{(4m+1)/3}. \tag{5.20}$$

The solution can then be marched forward in time using the algorithm just described.

6. Validation of the numerical method

Before using the procedure described in § 5 to compute flow solutions of general interest, the algorithm and implementation were tested against the asymptotic small-time solutions of § 4 and the experimental data of Keulegan & Carpenter (1958).

To compare with the small-time solutions of § 4 it was first necessary to compute solutions for $\omega_{\pm}(\tau)$ and $J_{\pm}$. This was done, for $c_0=0$, $\theta_0=\pi/2$, $\alpha_0=1$, $\beta_0=0$, $\vartheta_0=0$, and $m=0$, by solving the integro-differential equation (4.6) numerically using a method similar to that used by Pullin (1978). The corresponding numerical solutions for $\zeta_{\pm}(\Gamma,t)$ and $\Gamma_{\pm}(t)$ were then computed at the predetermined times $t_0=0$, $t_1=1/32$, $t_2=17/512$, $t_3=18/512$, ..., $t_{497}=1$ using the procedure described in § 5 with $c(t)=t$, $\theta(t)=\pi/2$, $\delta=0.2$, $J=514$, $P=16$, $Q=16$, $R=5/2$, and $T=11/2$. The two solutions, together with the small-time point-vortex solution from § 4, were then compared and the results are plotted in figures 4 and 5.

Figure 4(a) shows the small-time spiral-vortex solution for $\omega_{\pm}(\tau)$, which essentially coincides with that of Pullin (1978). Figure 4(b) shows the small-time point-vortex solution for $\Omega_{\pm}$ and figure 4(c) shows the numerical solution for $\zeta_{\pm}(\Gamma,t)$ at the times $t=1/4$, $t=1/2$, and $t=1$. The reader should note that in figure 4(c) the solutions for

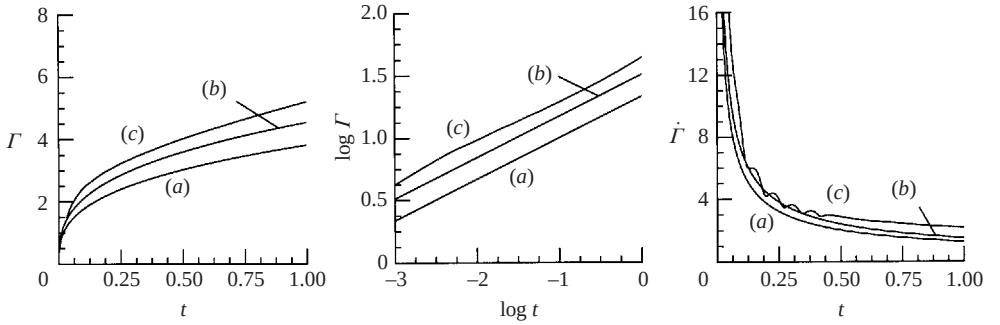

FIGURE 5. The impulsively started steady translation of a flat plate at constant angle of attack with $c(t)=t$ and $\theta(t)=\pi/2$. A comparison of $\Gamma_{\pm}(t)$ and $\dot{\Gamma}_{\pm}(t)$ for $t<1$ using (*a*) the small-time spiral-vortex solution, (*b*) the small-time point-vortex solution, and (*c*) the full numerical solution with $\delta=0.2$. The log–log plot of $\Gamma_{\pm}(t)$ confirms that $\Gamma_{\pm}(t)\sim t^{1/3}$.

$\zeta_{\pm}(\Gamma, t)$ have been self-similarly scaled, in line with equation (4.3), to aid comparison. Figure 5 shows the solutions for $\Gamma_{\pm}(t)$ and $\dot{\Gamma}_{\pm}(t)$ that correspond to each of the three types of solution mentioned above.

As the reader will note, there are slight discrepancies between the small-time spiral vortex solution and the full numerical solution. However, these discrepancies should not be unduly troubling; they are mainly due to the use of the point-vortex solution as an initial condition. The reader should also remember that δ is effectively zero in the small-time spiral-vortex solution whereas $\delta=0.2$ in the full numerical solution. What is more encouraging is that the three solutions for $\zeta_{\pm}(\Gamma, t)$ very nearly collapse onto the same curve when appropriately scaled. This shows that the algorithm and implementation are faithfully capturing the self-similar nature of the small-time solution. It is also worth mentioning that the oscillations in the time trace for $\dot{\Gamma}_{\pm}(t)$ are due to the roll-up of each new turn in the spiral vortex and should therefore not cause problems; once the spiral vortex has its specified number of turns, in this case five and a half, the oscillations disappear as expected.

We next consider a comparison with the experimental data of Keulegan & Carpenter (1958). The experiments in question were designed to measure the unsteady hydrodynamic forces on a submerged flat plate when placed in a family of time-periodic background flows. The wave-like background flows were chosen to produce as two-dimensional a flow field as possible and steps were taken to verify this assumption empirically. In fact, the authors claimed that the actual background flow was within 5% of the desired sinusoidally varying uni-directional background flow. The authors then measured the hydrodynamic forces on the submerged plate as a function of time and expressed the non-dimensional normal force as a modified Fourier series. The first five Fourier coefficients were then tabulated for each experimental run. The comparison presented here is for run number 42, in which the Reynolds number was 11400 and the Keulegan–Carpenter number was 3.8. The reader is reminded that the Keulegan–Carpenter number, denoted KC, is defined so that the non-dimensional period of oscillation is $2KC$.

The corresponding flow solution was then computed at the predetermined times $t_0=0$, $t_1=1/8$, $t_2=9/64$, $t_3=10/64, \ldots$ up until $t=2.5KC$ using the algorithm described in § 5 with $c(t)=-(KC/\pi)\cos(\pi t/KC)$, $\theta(t)=\pi/2$, $\delta=0.2$, $J=258$, $P=16$, $Q=16$, $R=5/2$, and $T=11/2$. Note that in the experiment the plate was held fixed while the fluid was moved. In the computation, the plate was moved through an

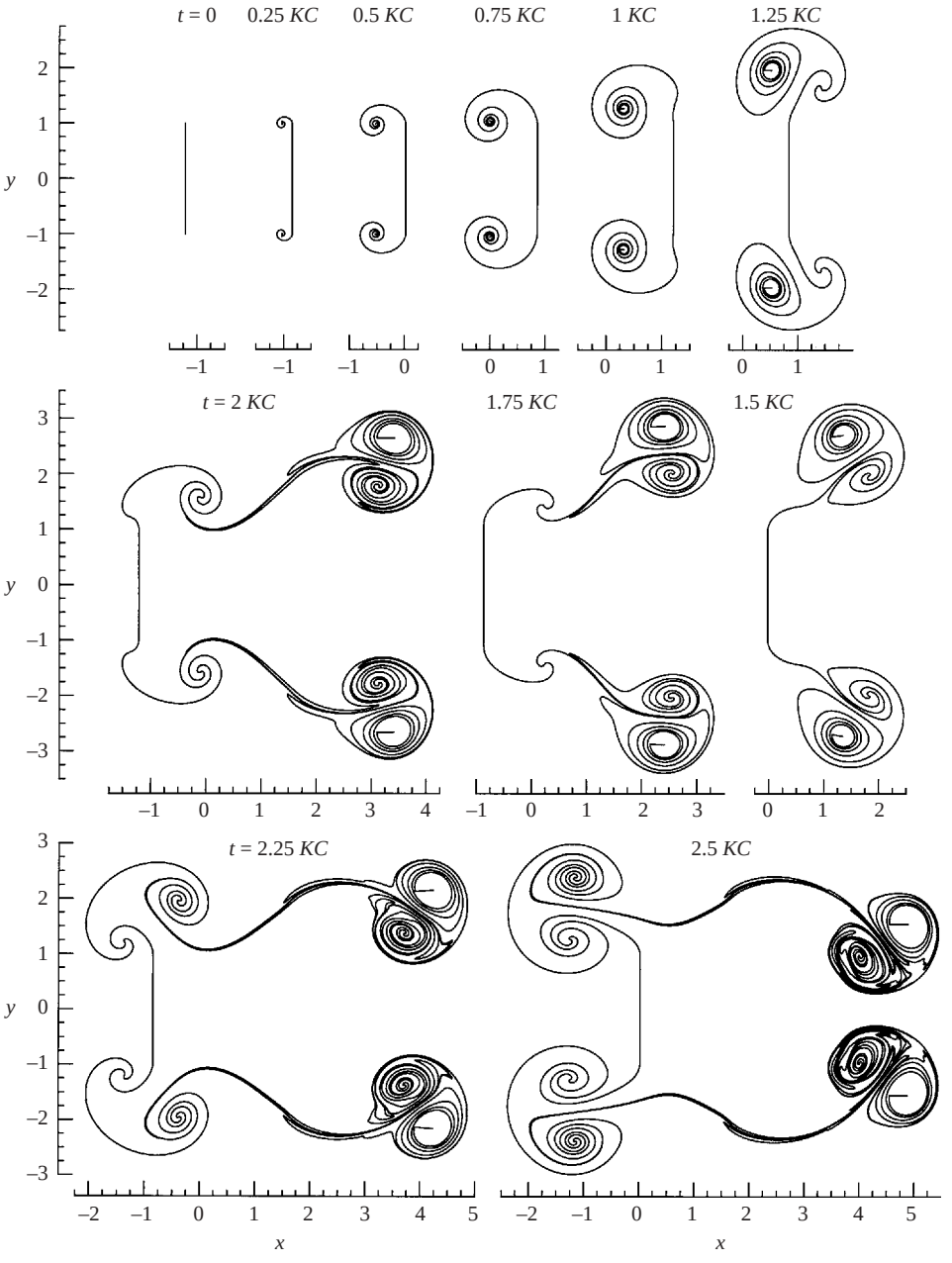

FIGURE 6. The wake induced by the sinusoidal oscillation of a flat plate in an otherwise stationary fluid with Keulegan–Carpenter number $KC = 3.8$, $c(t) = -(KC/\pi)\cos(\pi t/KC)$, and $\theta(t) = \pi/2$. The positions of the plate and the free vortex sheets $l_{\pm}(t)$ at times $t = 0$, $0.25KC$, $0.5KC$, $0.75KC$, $1KC$, $1.25KC$, $1.5KC$, $1.75KC$, $2KC$, $2.25KC$, and $2.5KC$.

otherwise undisturbed fluid. However, as far as the hydrodynamic forces on the plate are concerned, these two procedures are equivalent. The resulting flow solution is visualized in figure 6 by plotting the positions of the plate and the free vortex sheets at a number of different times throughout the first period of the motion. Figure 7 compares the computed normal force $\mathbb{F}(t)$ with the experimentally measured normal

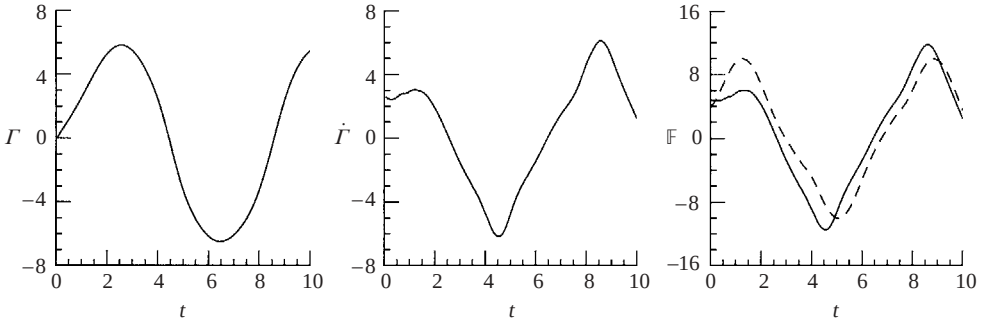

FIGURE 7. Comparison with the experimental data of Keulegan & Carpenter (1958). The computed edge circulations $\Gamma_{\pm}(t)$, shedding rates $\dot{\Gamma}_{\pm}(t)$, and total normal force $\mathbb{F}(t)$ over the first one and one quarter periods after start up from rest with Keulegan–Carpenter number $KC = 3.8$, $c(t) = -(KC/\pi)\cos(\pi t/KC)$, and $\theta(t) = \pi/2$. The experimentally measured normal force is shown as a broken line and represents a measurement taken well after start up from rest.

force; the experimental result of Keulegan & Carpenter (1958) is plotted as a broken line.

Before judging the comparison we should note two important points. First, that the computation was performed over the first one and a half periods of the oscillation, after start-up from rest. In contrast, the experimental measurements were taken once the flow had become time periodic. Second, we note that the flow around the experimental plate was almost certainly three-dimensional to some extent. Together these observations roughly account for the discrepancies between the two force traces in figure 7. For example, the fact that the computation was started from rest accounts for the large discrepancy between the two curves during the first half-period. This observation also goes some way to explaining the slight phase lag between the two curves. In any case, the agreement between the two force traces is surprisingly good.

Having successfully made the two comparisons outlined in this section we now move on to consider some other flows of interest, confident in the belief that the algorithm and implementation are performing correctly.

7. Results and discussion

We now present a number of numerical flow solutions that correspond to various prescribed motions of the plate. We begin with the relatively simple steady translation of the plate at constant angle of attack before moving on to consider some more complicated situations. In each example the structures in the wake of the plate are visualized by showing the positions of the free vortex sheets at several instants in time. The positions of the point vortices at the centre of each spiral are shown by connecting them to the free vortex sheets with a straight line. The edge circulations $\Gamma_{\pm}(t)$ are also plotted against time, as are the shedding rates $\dot{\Gamma}_{\pm}(t)$, the normal forces $\mathbb{F}_s(t)$, $\mathbb{F}_u(t)$, $\mathbb{F}_w(t)$, and $\mathbb{F}(t)$, and the torques $\mathbb{T}_s(t)$, $\mathbb{T}_u(t)$, $\mathbb{T}_w(t)$, and $\mathbb{T}(t)$.

All the featured solutions were computed at the predetermined times $t_0 = 0$, $t_1 = 1/16$, $t_2 = 5/64$, $t_3 = 6/64$, $t_4 = 7/64$, ... using the algorithm described in § 5 with $\delta = 0.2$ and $J = 66$. This value of J corresponds to a distribution of sixty-four points on the plate. In every example fourth-order Runge–Kutta time integration was used and direct summation was used in place of the more efficient fast summation algorithms for simplicity. New Lagrangian points were shed from each edge at every time step and adaptive point insertion was used with $P = 16$, $Q = 16$, $R = 5/2$, and $T = 11/2$.

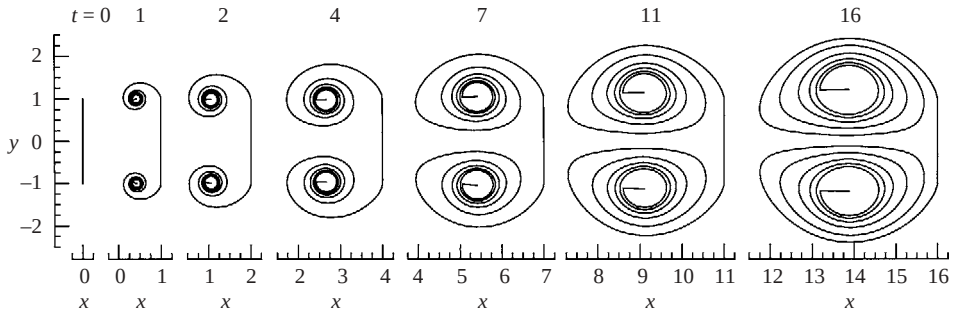

FIGURE 8. Example (*a*). The wake induced by the impulsively started steady translation of a flat plate at constant angle of attack with $c(t) = t$ and $\theta(t) = \pi/2$. The positions of the plate and the free vortex sheets $l_{\pm}(t)$ at times $t = 0$, 1, 2, 4, 7, 11, and 16.

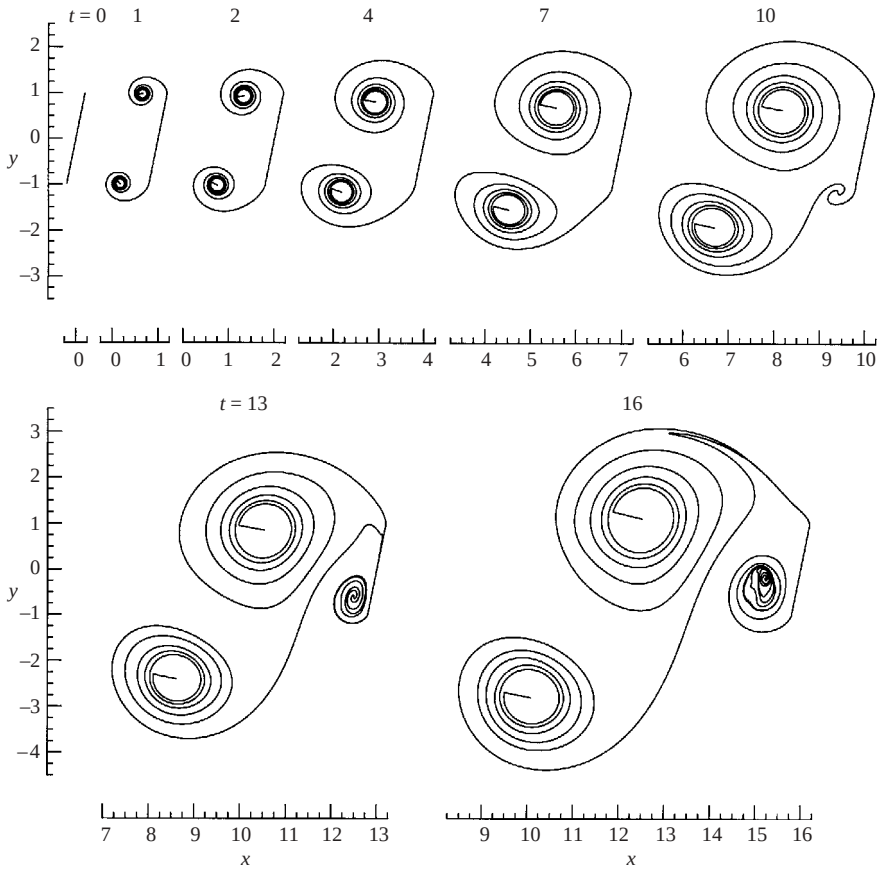

FIGURE 9. Example (*b*). The wake induced by the impulsively started steady translation of a flat plate at constant angle of attack with $c(t) = t$ and $\theta(t) = 7\pi/16$. The positions of the plate and the free vortex sheets $l_{\pm}(t)$ at times $t = 0$, 1, 2, 4, 7, 10, 13, and 16.

Although no convergence studies are presented it is stressed that all of the featured solutions are well resolved in both space and time.

In the first three examples presented (figures 8, 9 and 10) we study the impulsively started steady translation of a flat plate at constant angle of attack. As mentioned

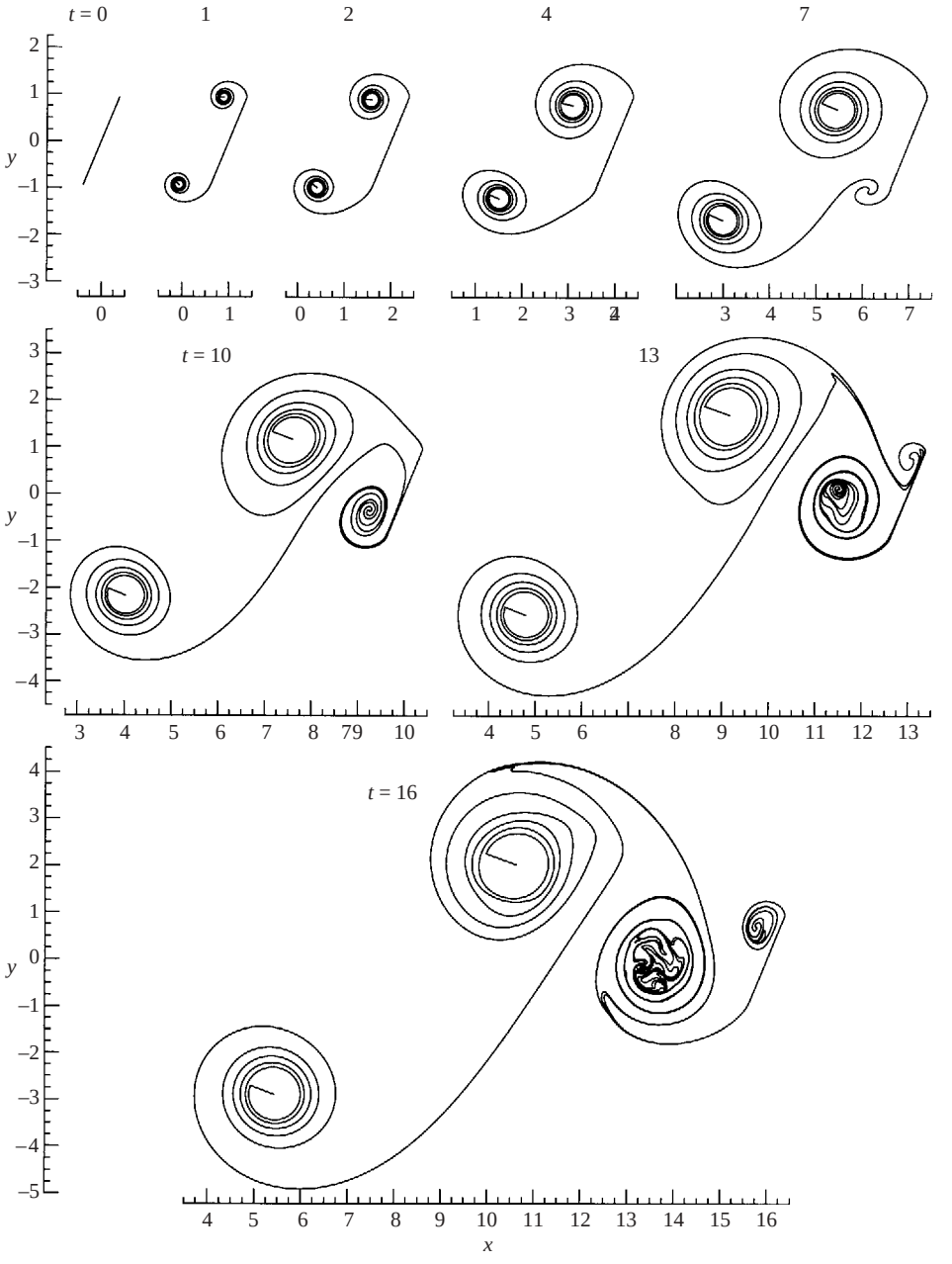

FIGURE 10. Example (*c*). The wake induced by the impulsively started steady translation of a flat plate at constant angle of attack with $c(t) = t$ and $\theta(t) = 3\pi/8$. The positions of the plate and the free vortex sheets $l_{\pm}(t)$ at times $t = 0$, 1, 2, 4, 7, 10, 13, and 16.

earlier the problem has been effectively non-dimensionalized based on U, the typical velocity of a point fixed in the plate, and so $c(t) = t$.

Example (*a*) is the symmetric case where $\theta(t) = \pi/2$. As expected the wake consists of the starting vortices that are produced impulsively at time $t = 0$. As time passes, these small starting vortices grow in size until they interact with each other and

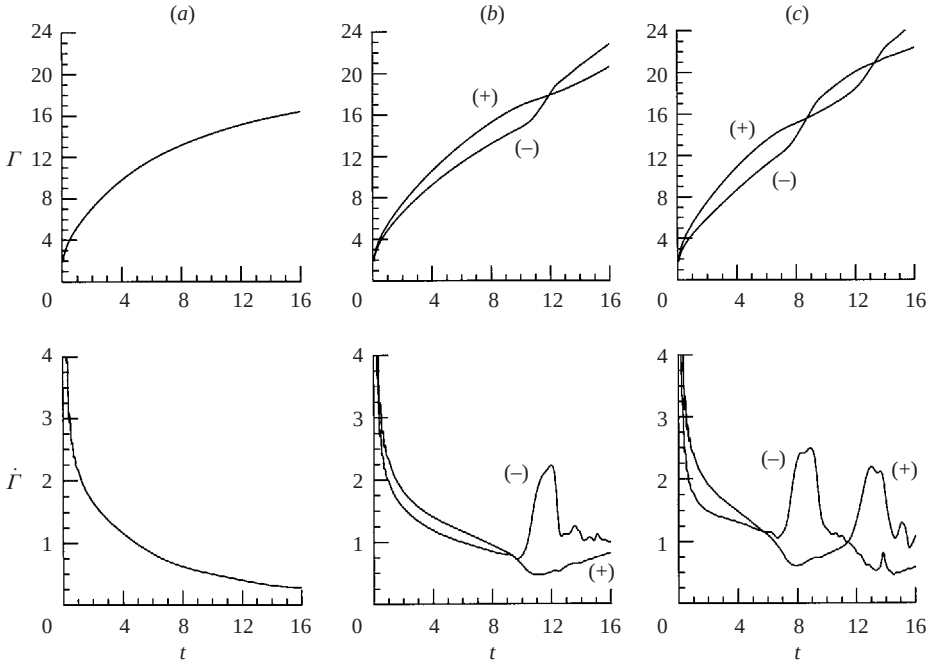

FIGURE 11. Examples (*a*), (*b*), and (*c*). The edge circulations $\Gamma_{\pm}(t)$ and the shedding rates $\dot{\Gamma}_{\pm}(t)$ that are induced by the impulsively started steady translation of a flat plate at constant angle of attack.

eventually approach an asymptotically steady-state configuration, see figure 8. We remark that this configuration is unlikely to remain stable in practice and is only observed in the calculation due to the exact symmetry of the solution algorithm. At the same time the circulation in each vortex, which is of equal magnitude and opposite sign, grows in time; initially growing as $t^{1/3}$ in line with the predictions of § 4, see figure 11(*a*). On the other hand, the total normal force $\mathbb{F}(t)$, which is composed almost entirely of its unsteady component $\mathbb{F}_u(t)$, decays in time. The torque, $\mathbb{T}(t)$, is zero as expected, see figure 12(*a*).

In example (*b*) a small degree of non-symmetry is introduced by decreasing the angle of attack to $\theta(t) = 7\pi/16$. We observe that until $t = 4$ the wake exhibits a structure not unlike that observed in example (*a*) and the normal force decays while the torque reaches a stable positive value, see figures 9 and 12(*b*). However, between $t = 4$ and $t = 8$ there is a significant growth in the bound circulation, $\Gamma_+(t) - \Gamma_-(t)$, and a corresponding growth in the steady component of the normal force $\mathbb{F}_s(t)$. The combination of these two effects gives rise to the characteristic plateau in the total normal force in figure 12(*b*).

Following this period of time the non-symmetry in the flow causes a new type of event to occur. Whilst the trailing-edge vortex is left slightly behind, the leading-edge vortex remains close to the plate and continues to grow in size. In fact, between $t = 7$ and $t = 10$ the leading-edge vortex grows so large that it begins to interfere with the shedding process at the trailing edge and a sharp increase in the rate at which circulation is shed from the trailing edge is observed, see figure 11(*b*). This extra circulation then rolls up into a new trailing-edge vortex, see figure 9. The formation of the new vortex is accompanied by a marked drop in $\mathbb{F}(t)$ followed by a strong

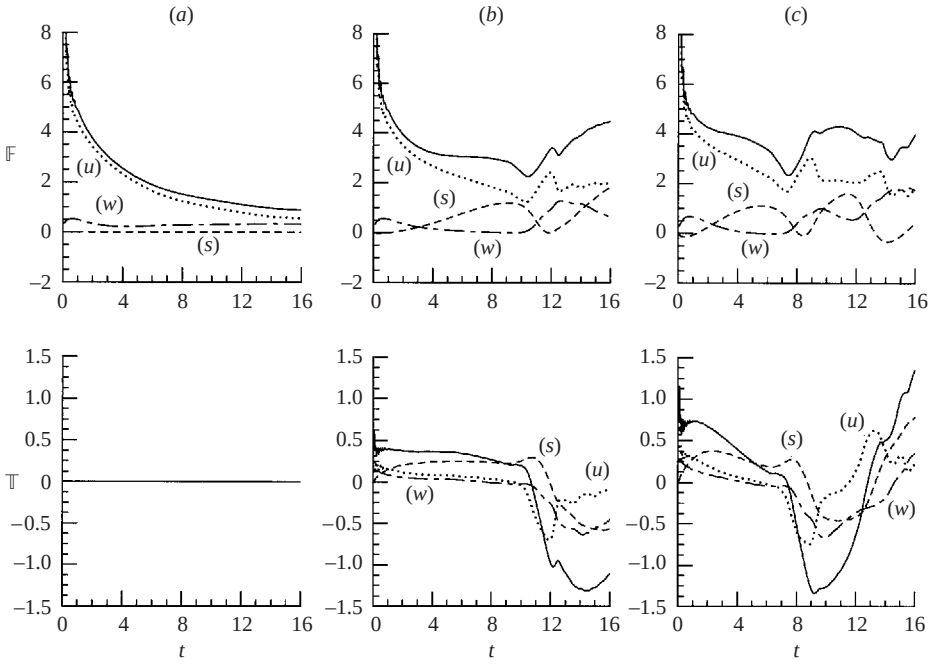

FIGURE 12. Examples (*a*), (*b*), and (*c*). The component forces $\mathbb{F}_s(t)$, $\mathbb{F}_u(t)$, and $\mathbb{F}_w(t)$, the total normal force $\mathbb{F}(t)$ (solid line), the component torques $\mathbb{T}_s(t)$, $\mathbb{T}_u(t)$, and $\mathbb{T}_w(t)$, and the total torque $\mathbb{T}(t)$ (solid line) that are induced by the impulsively started steady translation of a flat plate at constant angle of attack.

recovery. At the same time $\mathbb{T}(t)$ becomes sharply negative due to the low pressure in the core of the newly shed trailing-edge vortex, see figure 12(*b*).

In example (*c*) the angle of attack is further reduced to $\theta(t) = 3\pi/8$. As a result the new trailing-edge vortex is formed at an earlier time, somewhere between $t = 4$ and $t = 7$, see figure 10. Another difference is the subsequent formation of a new vortex at the leading edge, which appears between $t = 10$ and $t = 13$. This second shedding event is again accompanied by a peak in $\dot{\Gamma}_+(t)$, a marked drop in $\mathbb{F}(t)$, and a sharp change of sign in $\mathbb{T}(t)$. It is envisaged that this process of reciprocal vortex shedding will continue indefinitely leading to the eventual formation of a von Kármán vortex street in the wake. For a rudimentary description of this phenomenon see Sarpkaya (1975).

One other feature of note is the development of the complicated structure within the core of the newly shed trailing-edge vortex between $t = 13$ and $t = 16$. The solution remains well resolved during this period of time and an explanation for the development of the apparent complexity is offered in the recent work of Krasny & Nitsche (2002) on the chaotic dynamics of vortex sheet evolution.

We now move on to consider some more complicated examples in which the motion of the plate is determined by setting

$$c(t) = \frac{(t_1 + t_2)}{2} - \frac{\epsilon}{2}[2\log 2 + \log\cosh((t - t_1)/\epsilon) + \log\cosh((t - t_2)/\epsilon)], \tag{7.1}$$

and

$$\theta(t) = \frac{\pi}{2} + \frac{\epsilon\varphi}{(t_2 - t_1)}[\log\cosh((t - t_1)/\epsilon) - \log\cosh((t - t_2)/\epsilon)]. \tag{7.2}$$

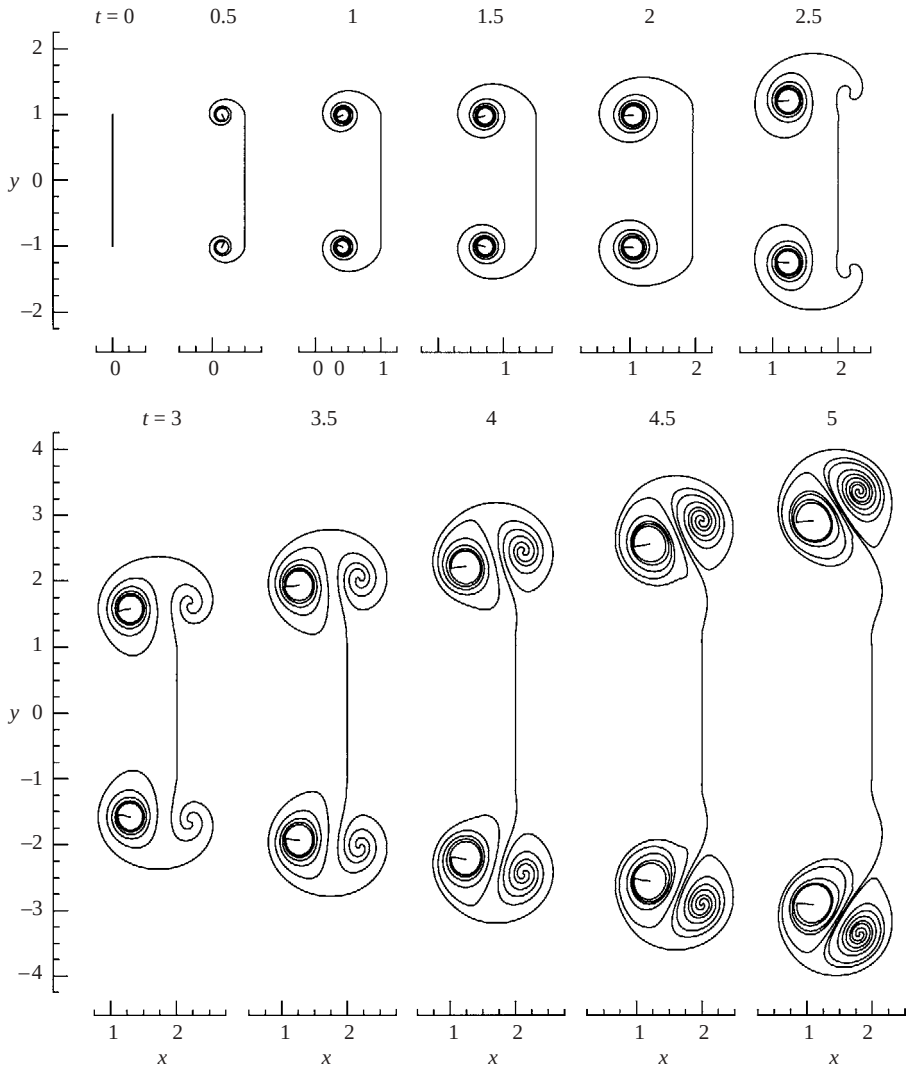

FIGURE 13. Example (*d*). The wake induced by the impulsively started and then smoothly stopped translation of a flat plate at constant angle of attack as defined by equations (7.1) and (7.2) with $t_1 = 2$, $t_2 = \infty$, $\epsilon = 1/8$, and $\varphi = 0$. The positions of the plate and the free vortex sheets $l_{\pm}(t)$ at times $t = 0$, 0.5, 1, 1.5, 2, 2.5, 3, 3.5, 4, 4.5, and 5.

The parameters t_1, t_2, ϵ, and φ are chosen so as to define a range of smooth motions that consist of a forward translation, followed by a smooth stop, a rotation, and finally a backward translation, shown in figures 13, 14 and 15. The motions are inspired by the movements of an insect wing during hovering flight, with particular reference to those portions of each wing beat where the wings are slowed, twisted, and then re-accelerated. However, the resulting motions are sufficiently generic to be of more general interest. The interested reader is referred to the experimental work of Dickinson & Gotz (1993) and Dickinson (1994) for a more biologically motivated study of the aerodynamics of insect flight.

In example (*d*) we consider the flow induced by a plate that is moved perpendicular to itself, through approximately one chord length, before being slowed and stopped at

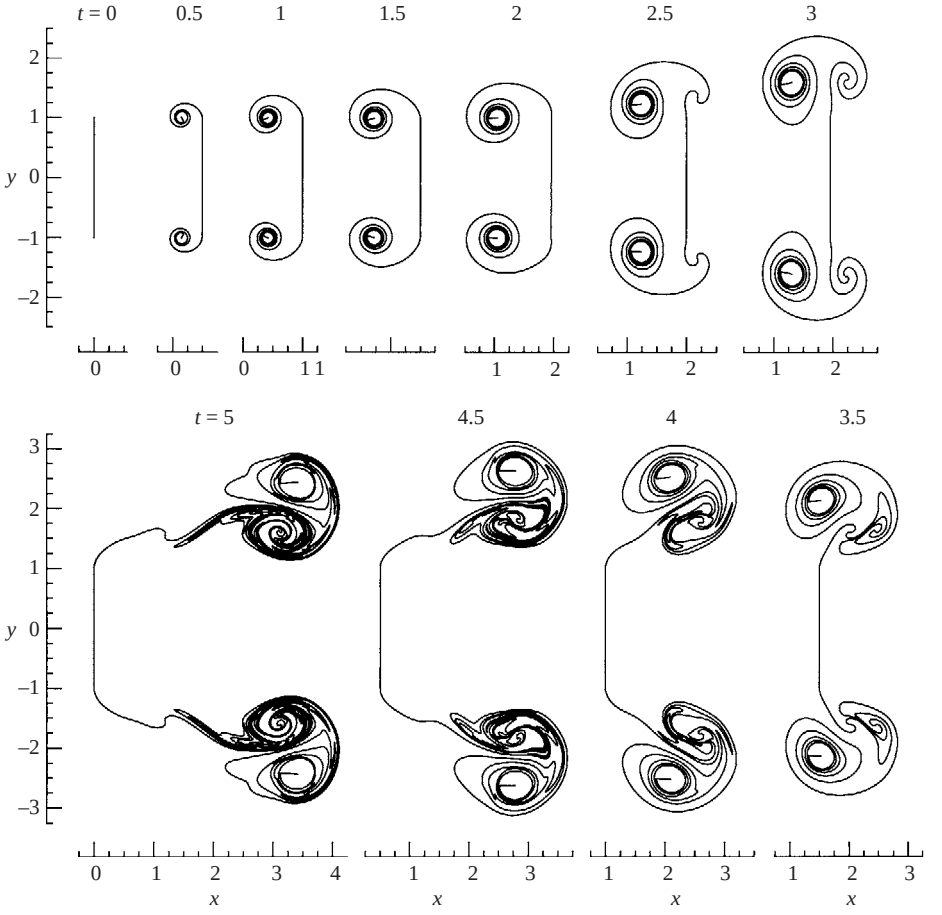

FIGURE 14. Example (*e*). The wake induced by the impulsively started, smoothly stopped, and smoothly reversed translation of a flat plate at constant angle of attack as defined by equations (7.1) and (7.2) with $t_1 = 2$, $t_2 = 3$, $\epsilon = 1/8$, and $\varphi = 0$. The positions of the plate and the free vortex sheets $l_{\pm}(t)$ at times $t = 0$, 0.5, 1, 1.5, 2, 2.5, 3, 3.5, 4, 4.5, and 5.

$t = 2$. The plate is then held still while the fluid continues to move. The flow solution is computed until $t = 5$. This motion is achieved by setting $t_1 = 2$, $t_2 = \infty$, $\epsilon = 1/8$, and $\varphi = 0$ in equations (7.1) and (7.2). The resulting wake is identical to that observed in example (*a*) until the stopping time $t = 2$ at which point two stopping vortices are formed, see figure 13.

The formation of the stopping vortices is again accompanied by a sharp peak in the rate of shedding, this time with negative sign, and by a corresponding drop in $\mathbb{F}(t)$, which closely follows the behaviour of $\dot{\Gamma}_{\pm}(t)$. See figures 16(*d*) and 17(*d*). After the plate has stopped the stopping vortices continue to grow in size and quickly pair up with their corresponding starting vortices to form two dipolar structures. Since the starting vortices have slightly more circulation than the stopping vortices, due to the impulsive nature of their creation, the dipoles move off to the left along curved trajectories while $\mathbb{F}(t)$ and $\dot{\Gamma}_{\pm}(t)$ decay in time.

In example (*e*), the plate is not only slowed and stopped but is also moved back to its original position. The motion is achieved by setting $t_1 = 2$, $t_2 = 3$, $\epsilon = 1/8$, and $\varphi = 0$ in equations (7.1) and (7.2). The resulting flow is identical to that of example (*d*) until

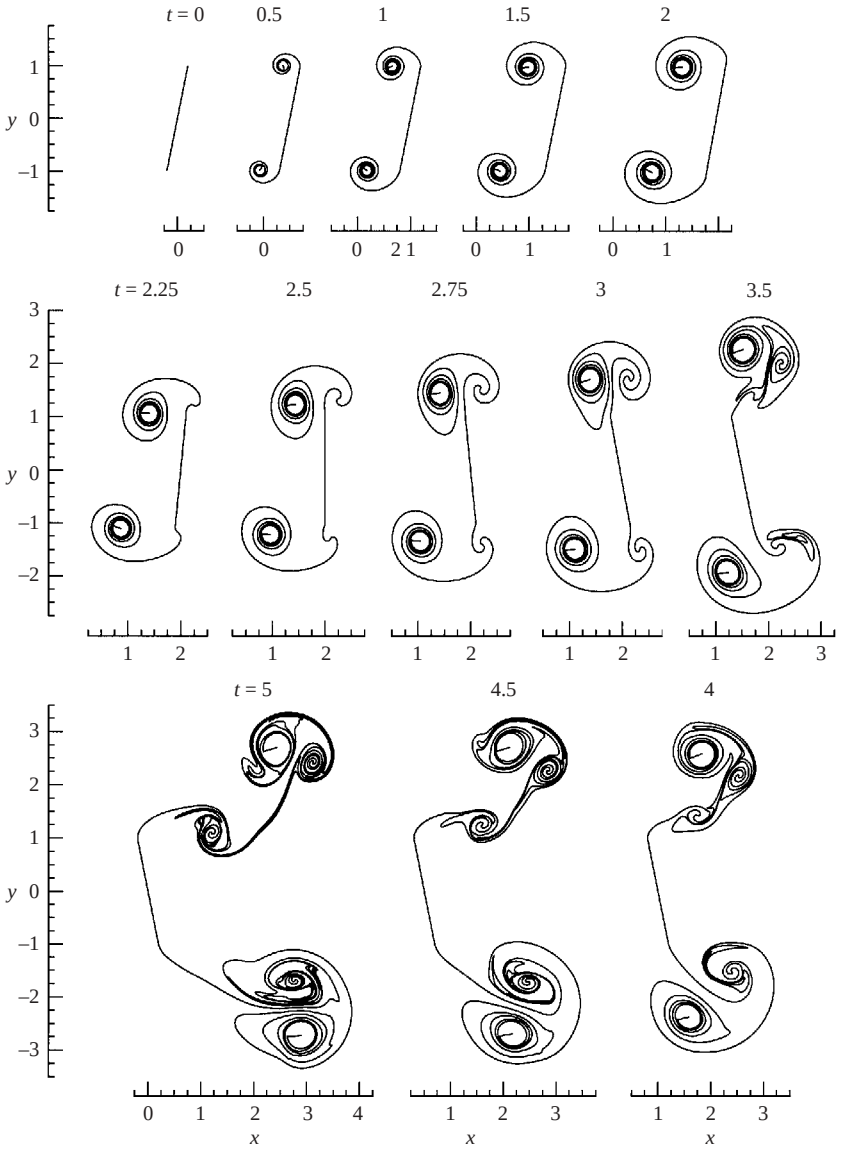

FIGURE 15. Example (f). The wake induced by the impulsively started, smoothly stopped, and smoothly reversed translation of a flat plate with varying angle of attack as defined by equations (7.1) and (7.2) with $t_1 = 2$, $t_2 = 3$, $\epsilon = 1/8$, and $\varphi = \pi/16$. The positions of the plate and the free vortex sheets $l_{\pm}(t)$ at times $t = 0$, 0.5, 1, 1.5, 2, 2.25, 2.5, 2.75, 3, 3.5, 4, 4.5, and 5.

the restarting time $t = 3$ at which point two more starting vortices are formed. The new vortices join with and strengthen the existing stopping vortices, which then again pair up with the original starting vortices to form two complicated dipolar structures. See figure 14. As a result a second negative peak is produced in both $\mathbb{F}(t)$ and $\dot{\Gamma}_{\pm}(t)$ at $t = 3$, see figures 16(e) and 17(e). In the remainder of the calculation the dipolar structures move off to the right as the plate moves back to the left and, since the shedding rates remain relatively high, some extra circulation is shed and rolls up into the beginnings of two new vortices.

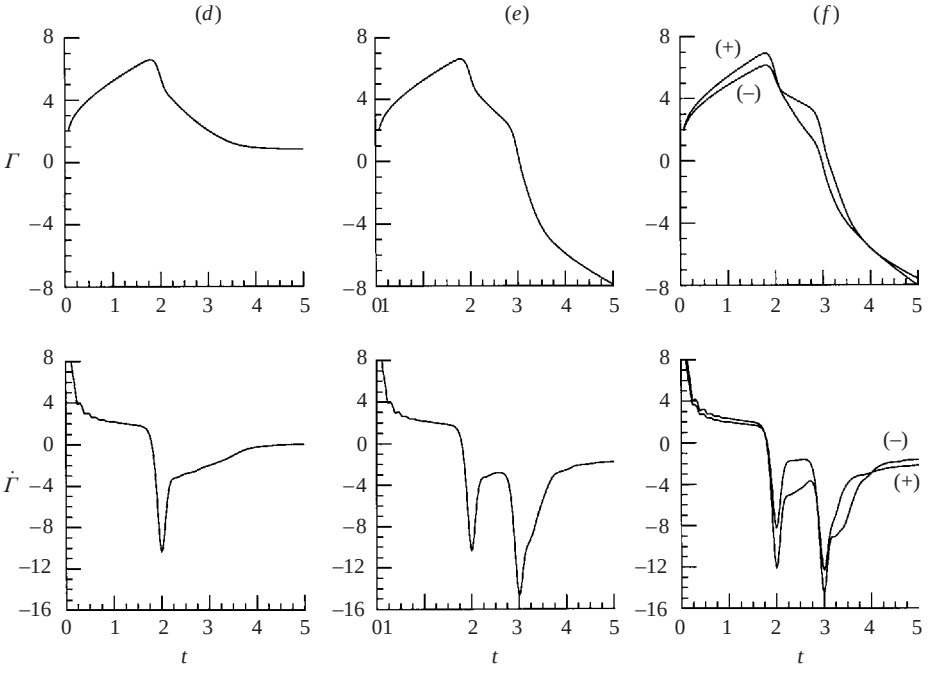

FIGURE 16. Examples (*d*), (*e*), and (*f*). The edge circulations $\Gamma_{\pm}(t)$ and the shedding rates $\dot{\Gamma}_{\pm}(t)$ that are induced by the unsteady oscillation of a plate. The exact motions of the plate are described fully in the text.

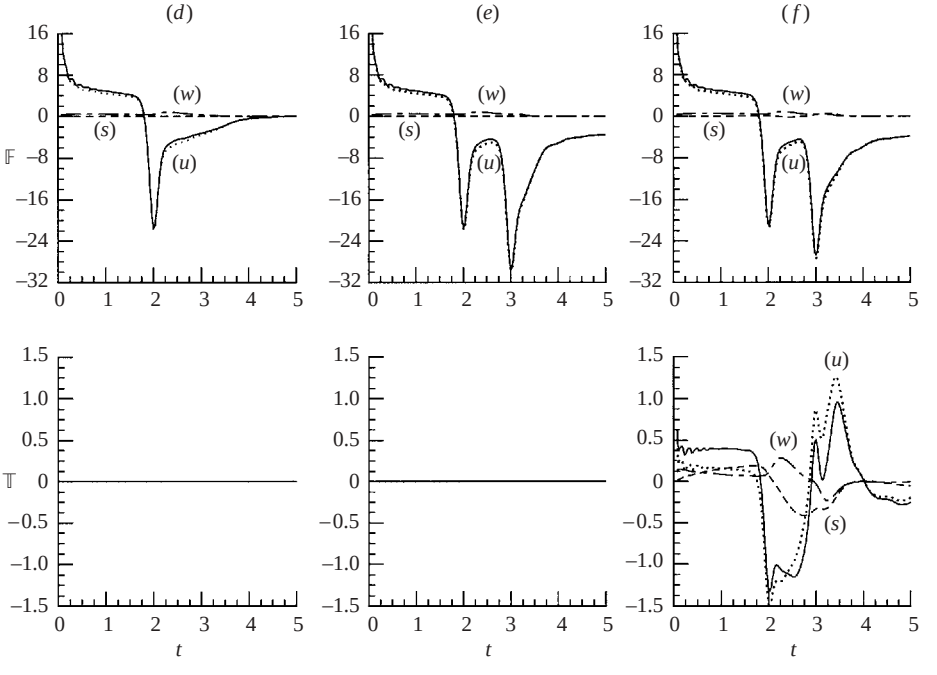

FIGURE 17. Examples (*d*), (*e*), and (*f*). The component forces $\mathbb{F}_s(t)$, $\mathbb{F}_u(t)$, and $\mathbb{F}_w(t)$, the total normal force $\mathbb{F}(t)$, the component torques $\mathbb{T}_s(t)$, $\mathbb{T}_u(t)$, and $\mathbb{T}_w(t)$, and the total torque $\mathbb{T}(t)$ that are induced by the unsteady oscillation of a plate.

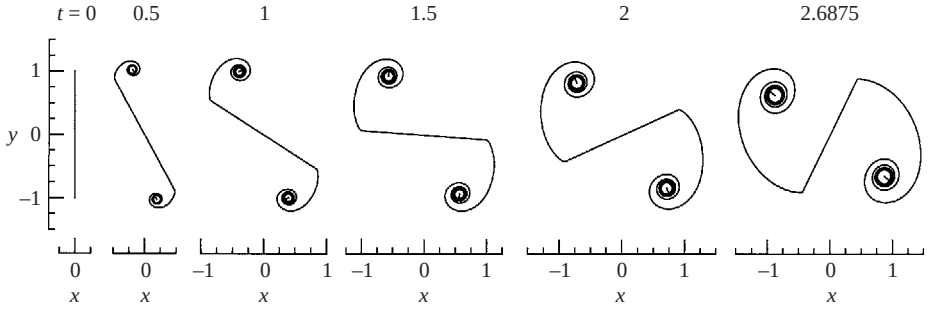

FIGURE 18. The wake induced by the impulsively started steady rotation of a flat plate with $c(t)=0$ and $\theta(t)=t$. The positions of the plate and the free vortex sheets $l_{\pm}(t)$ at times $t=0$, 0.5, 1, 1.5, 2, and the catastrophic time $t^* \approx 2.6875$.

In the final case, example (f), a small degree of non-symmetry is added by superposing an unsteady rotation on top of the motion presented in example (e). The motion, which is achieved by setting $t_1=2$, $t_2=3$, $\epsilon=1/8$, and $\varphi=\pi/16$ in equations (7.1) and (7.2), then begins to resemble the motion of an insect wing during hovering flight. However, since the degree of non-symmetry remains slight, the normal forces and shedding rates remain similar to those observed in example (e). On the other hand, the structures in the wake are markedly different. For example the upper and lower dipolar structures produced on the return stroke are of differing size and move off in differing directions while a strong new leading-edge vortex is formed at around $t=4$. In addition we note that an overall positive lift is produced in example (f) in contrast with the pure drag produced in examples (d) and (e).

7.1. *Limitations of the numerical method*

The solutions presented so far are restricted to situations that exhibit high effective angles of attack. This is because the current numerical method is unable to cope consistently with situations at lower angles of attack due to the occurrence of a specific type of event. The event in question occurs if either of the inequalities

$$\mu(c_+,t)-\tau(t)>0 \quad \text{or} \quad \mu(c_-,t)-\tau(t)<0 \tag{7.3}$$

become not satisfied at some finite time t^* and corresponds physically to a situation in which a newly shed Lagrangian fluid particle begins to move onto instead of away from the plate. A Lagrangian particle finding itself in such a predicament would be forced to remain on the plate, as a consequence of the no-penetration boundary condition, and it is this that leads to a catastrophe as far as further time-integration of governing equations is concerned.

In fact, to make matters worse the same problem can also occur at high effective angles of attack in situations where the plate is forced to interact with its own wake. The simplest example that fits the description is the impulsively started steady rotation of a flat plate, see figure 18. The motion is determined by setting $c(t)=0$ and $\theta(t)=t$. As expected, two initial starting vortices are shed from plate's edges at $t=0$ and continue to grow in time. However, since the plate is rotating these starting vortices are not left behind but remain in the vicinity of the plate until they grow so large that they interfere with the shedding process at the opposite edge. Conditions (7.3) first become not satisfied at $t^* \approx 2.6875$ and the flow solution cannot be computed beyond this time using the current numerical method. The author is currently developing a new approach to deal with such situations.

8. Conclusions

In summary, we have successfully modelled the separated flow of an inviscid fluid around a moving flat plate using a boundary integral representation for the complex-conjugate velocity field $\Phi(z,t)$. Starting from an ansatz for $\Phi(z,t)$ we then systematically derived a system of governing evolution equations for the problem which ensured that all the required boundary conditions were automatically satisfied. As part of this derivation the unsteady Kutta condition was rigorously imposed in the form of two new integral constraints, see equation (3.13), from which all of the conditions traditionally associated with the imposition of the steady Kutta condition were derived. Furthermore, the extensive use of Chebyshev polynomial expansions lead to the derivation of explicit expressions for the normal force and torque on the plate, see equations (3.37) and (3.38), which will provide unique insight into the high-lift mechanisms of two-dimensional unsteady aerodynamics. Finally, a novel numerical treatment of the full problem was proposed and implemented and the results of several example calculations were presented.

The results presented showed several interesting features, the most noteworthy of which was that much larger aerodynamic loads were produced in the unsteady context than with the steady situation. However, an extensive investigation of differing plate motions is required before more concrete statements can be made on the subject.

As a final comment we remark that generalizations of the theory presented here are currently under investigation by the author, including the introduction of plate flexibility, aerodynamic feedback, gravity, active control, and three-dimensionality.

I would like to thank Professors Steve Childress, Mike Shelley, and Robert Krasny for their many enlightening conversations and comments during the preparation of this manuscript.

Appendix A

The following is a list of identities that prove useful in the derivations presented in the body of the paper and expressed in the same notation:

$$\frac{\mathrm{i}\,\mathrm{e}^{-\mathrm{i}\theta(t)}}{\pi}\int\limits_{l_=(t)}\frac{\sqrt{\lambda-c_+}\sqrt{\lambda-c_-}}{(\lambda-\zeta)}\,\mathrm{d}\lambda = s(\zeta,t),$$

$$\frac{\mathrm{i}\,\mathrm{e}^{-\mathrm{i}\theta(t)}}{\pi}\int\limits_{l_=(t)}\frac{\sqrt{\lambda-c_+}\sqrt{\lambda-c_-}}{(\lambda-\zeta)}s(\lambda,t)\,\mathrm{d}\lambda = \tfrac{1}{2}-r^2(\zeta,t),$$

$$\frac{\mathrm{i}\,\mathrm{e}^{-\mathrm{i}\theta(t)}}{\pi}\int\limits_{l_=(t)}\frac{\sqrt{\lambda-c_+}\sqrt{\lambda-c_-}}{(\lambda-\zeta)}\,U_{n-1}(s(\lambda,t))\,\mathrm{d}\lambda = T_n(s(\zeta,t)),$$

$$\frac{\mathrm{i}\,\mathrm{e}^{-\mathrm{i}\theta(t)}}{\pi}\int\limits_{l_=(t)}\frac{\sqrt{\lambda-c_+}\sqrt{\lambda-c_-}}{(\lambda-\zeta)}\log|\lambda-c_\pm|\,\mathrm{d}\lambda = \mp 1-\log(2)s(\zeta,t)\mp\pi a_\pm(s)r(\zeta,t),$$

$$\frac{\mathrm{i}}{\pi}\int\limits_{l_=(t)}\frac{\sqrt{\lambda-c_+}\sqrt{\lambda-c_-}}{(\lambda-\zeta)(z-\lambda)}\,\mathrm{d}\lambda = \frac{\sqrt{z-c_+}\sqrt{z-c_-}}{(z-\zeta)}-1,$$

$$\frac{\sqrt{z-c_+}\sqrt{z-c_-}}{(z-\zeta)} = \frac{1}{\sqrt{z-c_+}\sqrt{z-c_-}}\left[(z-c)+(\zeta-c)+\frac{(\zeta-c_+)(\zeta-c_-)}{(z-\zeta)}\right].$$

Appendix B

This appendix contains two asymptotic expansions that detail the leading-order behaviour of particular Cauchy integrals for z near $c_{\pm}(t)$. The expansions are written in the notation of the paper except that here $l_{=}(t)$ is not necessarily a straight line segment. In each case the next term in the asymptotic expansion remains of order unity as z approaches $c_{\pm}(t)$. A full and more general account is given in Muskhelishvili (1946, chap. 4).

$$\int_{l_{=}(t)} \frac{\phi(\lambda, t)}{(\lambda - z)}\,\mathrm{d}\lambda \sim \pm\phi(c_{\pm}, t)\log(z - c_{\pm}) + \cdots \quad \text{for} \quad z \sim c_{\pm}(t),$$

$$\int_{l_{=}(t)} \frac{\phi(\lambda, t)\,\mathrm{d}\lambda}{\sqrt{\lambda - c_{+}}\sqrt{\lambda - c_{-}}(\lambda - z)} \sim \frac{\mathrm{i}\pi\phi(c_{\pm}, t)}{\sqrt{z - c_{\pm}}\sqrt{c_{\pm} - c_{\mp}}} + \cdots \quad \text{for} \quad z \sim c_{\pm}(t).$$

REFERENCES

Birkhoff, G. 1962 Helmholtz and Taylor instability. *Proc. Symp. in Applied Mathematics*, vol. XIII. Am. Math. Soc.

Chorin, A. L. & Bernard, P. S. 1973 Discretisation of a vortex sheet, with an example of roll-up. *J. Comput. Phys.* **13**, 423–429.

Clements, R. R. 1973 An inviscid model of two-dimensional vortex shedding. *J. Fluid Mech.* **57**, 321–336.

Cortelezzi, L., Chen, Y. C. & Chang, H. L. 1997 Nonlinear feedback control of the wake past a plate: From a low-order model to a high-order model. *Phys. Fluids* **9**, 2009–2021.

Cortelezzi, L. & Leonard, A. 1993 Point vortex model of the unsteady separated flow past a semi-infinite plate with transverse motion. *Fluid Dyn. Res.* **11**, 263–295.

Dickinson, M. H. 1994 The effects of wing rotation on unsteady aerodynamic performance at low Reynolds numbers. *J. Expl Biol.* **192**, 179–206.

Dickinson, M. H. & Gotz, K. G. 1993 Unsteady aerodynamic performance of model wings at low Reynolds numbers. *J. Expl Biol.* **174**, 45–64.

Didden, N. 1979 On the formation of vortex rings: rolling-up and production of circulation. *Z. Angew. Math. Phys.* **30**, 101.

Draghicescu, C. I. & Draghicescu, M. 1995 A fast algorithm for vortex blob interactions. *J. Comput. Phys.* **116**, 69–78.

Fage, A. & Johansen, F. C. 1927 On the flow of air behind an inclined flat plate of infinite span. *Proc. R. Soc. Lond.* A **116**, 170.

Greengard, L. & Rokhlin, V. 1987 A fast algorithm for particle simulations. *J. Comput. Phys.* **73**, 325–348.

Katz, J. 1981 A discrete vortex method for the non-steady separated flow over an airfoil. *J. Fluid Mech.* **102**, 315–328.

Keulegan, G. H. & Carpenter, L. H. 1958 Forces on cylinders and plates in an oscillating fluid. *J. Res. Natl Bureau Standards* **60**, 423–440.

Krasny, R. 1986*a* Desingularisation of periodic vortex sheet roll-up. *J. Comput. Phys.* **65**, 292–313.

Krasny, R. 1986*b* A study of singularity formation in a vortex sheet by the point-vortex approximation. *J. Fluid Mech.* **167**, 65–93.

Krasny, R. 1987 Computation of vortex sheet roll-up in the Trefftz plane. *J. Fluid Mech.* **184**, 123–155.

Krasny, R. 1991 Vortex sheet computations: roll-up, wakes, separation. *Lectures in Applied Mathematics. Am. Math. Soc.* **28**, 385–401.

Krasny, R. & Nitsche, M. 2002 The onset of chaos in vortex sheet flow. *J. Fluid Mech.* **454**, 47–69.

Kuwahara, K. 1973 Numerical study of flow past an inclined flat plate by an inviscid model. *J. Phys. Soc. Japan* **35**, 1545.

Moore, D. W. 1974 A numerical study of the roll-up of a finite vortex sheet. *J. Fluid Mech.* **63**, 225–235.

Moore, D. W. 1975 The rolling up of a semi-infinite vortex sheet. *Proc. R. Soc. Lond.* A **345**, 417–430.

Moore, D. W. 1979 The spontaneous appearance of a singularity in the shape of an evolving vortex sheet. *Proc. R. Soc. Lond.* A **365**, 105.

Muskhelishvili, N. I. 1946 *Singular Integral Equations.* Moscow.

Nitsche, M. & Krasny, R. 1994 A numerical study of vortex ring formation at the edge of a circular tube. *J. Fluid Mech.* **97**, 239–255.

Prandtl, L. & Tietjens, O. G. 1934 *Fundamentals of Hydro- and Aeromechanics.* Republished by Dover in 1957.

Pullin, D. I. 1978 The large-scale structure of unsteady self-similar rolled up vortex sheets. *J. Fluid Mech.* **88**, 401–430.

Pullin, D. I. & Perry, A. E. 1980 Some flow visualisation experiments on the starting vortex. *J. Fluid Mech.* **97**, 239–255.

Rott, N. 1956 Diffraction of a weak shock with vortex generation. *J. Fluid Mech.* **1**, 111–128.

Saffman, P. G. 1992 *Vortex Dynamics.* Cambridge University Press.

Sarpkaya, T. 1975 An inviscid model of two-dimensional vortex shedding for transient and asymptotically steady separated flow over an inclined plate. *J. Fluid Mech.* **68**, 109–128.

Sarpkaya, T. 1989 Computational methods with vortices – The 1988 Freeman Scholar lecture. *Trans. ASME*: *J. Fluids Engng Trans.* **111**, 5–52.

Taneda, S. & Honji, H 1971 Unsteady flow past a flat plate normal to the direction of motion. *J. Phys. Soc. Japan* **30**, 262–272.